Uniform Practical Asymptotic Stability for Position Control of Underwater Snake Robots

Amer Orucevic, *Graduate Student Member, IEEE*, Marianna Wrzos-Kaminska, Jan Tommy Gravdahl, *Senior Member, IEEE*, and Kristin Y. Pettersen, *Fellow, IEEE*

***Abstract*— In this paper, Lyapunov theory for uniform practical asymptotic stability (UPAS) is presented and utilized to solve the problem of position control of a planar underwater snake robot (USR). First sufficient conditions for UPAS of a time-varying nonlinear system and a theorem for UPAS of cascaded systems are presented. These are then utilized to design controllers that stabilize the position of an USR when approaching from such a direction that the USR moves against the current. A simulation study of the controller applied to the ideal case is then studied to investigate how the controller performs. Then the theoretical results are validated through a high-fidelity simulation study.**

***Index Terms*— Autonomous underwater vehicles, nonlinear systems, snake robots, stability analysis**

I. INTRODUCTION

Our understanding of the oceans is crucial for meeting challenges such as food sufficiency, bio-diversity, renewable energy, transport, and access to minerals and other resources. To fully access the vast oceans we need efficient, autonomous marine robots. One promising approach is underwater snake robots (USRs), which are autonomous underwater vehicles (AUVs) consisting of several slim segments connected by joints. The advantage of this design is that it allows the USR to access narrow spaces while moving by mimicking an eel [1], and to interact with its environment in the same way as a traditional robotic manipulator arm.

Power delivery remains a challenge for AUVs. Battery constraints limit their operational time, while tethers would limit their operational area and autonomy. Improving the energy efficiency of these systems would be a significant step forward in our attempts to design efficient AUVs. We want to pursue the idea of achieving energy autonomy by utilizing the energy in waves, currents and other hydrodynamic effects such as wakes behind bluff bodies [2], [3]. To this end, we aim to develop a controller that allows the USR to hold a desired position with an undulatory motion, downstream from a bluff body. As a first step to achieving this, we present a controller that stabilizes the position of a planar-USR with an undulatory motion when moving against a time-varying current.

Various control strategies have been developed and studied for the undulatory motion of snake robots. The line-of-sight (LOS) guidance control law was implemented for terrestrial snake robots in [4], and also for USRs in [1]. However, those approaches are not suitable in the presence of environmental disturbances such as currents. To address this, the integral line-of-sight (ILOS) guidance control law was proposed for USRs in [5]. In [6], the ILOS guidance law was shown to provide semi-global exponential stability, under the assumption that the forward velocity is always greater than the velocity of the current. However, stabilizing the position of the USR requires that these velocities are equal. Direction following control of the terrestrial snake robot is studied in [7], by using virtual holonomic constraints (VHCs) to encode a sinusoidal gait pattern for forward propulsion. This was done by utilizing hierarchical control design [8]. A similar approach was later used to design maneuvering controllers for both terrestrial snake robots [9] and USRs [10]. Our goal is for the USR to operate in the wake of a bluff body, where the environmental forces are time-varying, which results in reference signals and disturbances that are time-dependent. The controllers developed in [9], [10], however, assume that the systems are time-invariant. To address this issue, in this paper the control approach and corresponding stability proofs are extended to time-varying systems. Additionally, to achieve a desired orientation that drives the USR towards a reference position, a guidance law is proposed that generates an angular velocity reference. However, the controllers presented in [9], [10] are designed for a desired heading angle. The controllers in this paper are therefore adapted for angular velocity tracking.

The guidance law proposed in this paper is inspired by the approaches taken in [11]–[13] where a geometric controller is developed and studied for position tracking of quad-copters in three dimensions [11], [12]. This was later adapted for the path-following of underactuated autonomous surface vessels (ASVs) and AUVs moving in a plane [13]. For our purposes the guidance law has been adapted for the position tracking of planar USRs, by including a reference velocity along the y-axis in addition to the reference velocity along the x-axis used in [13]. The reference velocities are then designed to stabilize the position of the USR.

The stability analysis in [7], [9], [10] is based on hierarchi-

This project has received funding from the European Research Council (ERC) under the European Union's Horizon 2020 research and innovation programme, through the ERC Advanced Grant 101017697-CRÈME. The work is also supported by the Research Council of Norway through the Centres of Excellence funding scheme, project No. 223254 – NTNU AMOS and project No. 304667.

A. Orucevic, M. Wrzos-Kaminska, J. T. Gravdahl, K. Y. Pettersen are with the Centre for Autonomous Marine Operations and Systems, Department of Engineering Cybernetics, Norwegian University of Science and Technology (NTNU), Trondheim, Norway {Amer.Orucevic, Marianna.Wrzos-Kaminska, Tommy.Gravdahl, Kristin.Y.Pettersen}@ntnu.no

cal control design [8], which requires time-invariant systems and is therefore not applicable in our case, where a time-varying current is to be considered. Instead, we utilize cascaded systems theory, which has proved to be an efficient tool for analyzing the stability of nonlinear dynamical systems [14], [15]. For time-varying nonlinear systems, cascaded systems theory is well established for cascades of uniformly asymptotically stable systems; uniformly globally asymptotically stable (UGAS) systems [15], uniformly semi-globally asymptotically stable (USAS) systems [16] and locally uniformly asymptotically stable (UAS) systems [17].

However, in the presence of nonvanishing perturbations such as modeling errors, unmodelled disturbances and measurement noise, asymptotic stability may not be attainable. In these cases the system may not converge to the origin but rather to some neighborhood of the origin. When that neighborhood can be diminished at will by the choice of parameters, this is referred to as uniform global practical asymptotic stability (UGPAS). In [16] it is shown that a cascaded system consisting of two UGPAS systems with uniformly bounded (UB) solutions retains the UGPAS property. Moreover, Lyapunov sufficient conditions for UGPAS are proposed and proven. The global requirements of UGPAS can be alleviated by considering uniform semi-global practical asymptotic stability (USPAS). This has been studied in [18] where Lyapunov sufficient conditions and the stability of cascades of USPAS systems were proven. However, USPAS requires that the region of attraction can be enlarged to any desirable size by the choice of parameters. The guidance laws and controllers in [11]–[13] give almost-GAS and put constraints on the desired velocities of the vehicles, and therefore achieving either global or semi-global stability is not possible. The strongest stability property we may hope to establish for the resulting closed-loop system is thus local uniform practical asymptotic stability (UPAS) as presented in [19]. This is a special case of USPAS where the region of attraction is not required to be arbitrarily enlargeable. A corollary is also presented with conditions for a time-varying nonlinear system to be UPAS in [19].

In this paper we establish Lyapunov sufficient conditions for the UPAS of time-varying nonlinear systems as well as for cascades of such systems. We then apply these to show the UPAS of the closed-loop system, proving that the proposed control law stabilizes the position of the USR with an undulatory motion in the presence of time-varying disturbances when moving against a constant current along the x-axis. Preliminary results were presented in [20], where a sketch of the proofs was presented and a Matlab simulation study was performed. In this paper we extend the previous results with complete proofs of the theorems presented. Moreover, we perform a high-fidelity simulation study using the coupled solver presented by [2], and the controllers are adjusted to improve performance. Additionally, the assumptions made for a cascaded system to be UPAS are relaxed by removing the assumption that the solutions of the complete system have to be bounded, instead showing that this follows from the other assumptions made.

The paper is organized as follows: In Section II the notation used in this paper is presented. Then in Section III we present the precise definition of UPAS as we use it. Furthermore, sufficient conditions for UPAS of a time-varying dynamical system and a theorem for UPAS of cascaded systems are presented. In Section IV the control objectives and a control-oriented model of an USR are presented. The controllers and guidance law proposed in this paper are then presented in Section V, with an analysis of the resulting closed-loop system. Then the simulation setup and results are presented in Section VII. Finally, in Section IX conclusions are given.

II. Preliminaries

A class $\mathcal{K}$ function is a continuous function $\alpha : \mathbb{R}_{\geq 0} \to \mathbb{R}_{\geq 0}$ that is strictly increasing and satisfies $\alpha(0) = 0$. If additionally $\alpha(s) \to \infty$ when $s \to \infty$ then $\alpha \in \mathcal{K}_\infty$. A class $\mathcal{L}$-function is a continuous function $\sigma : \mathbb{R}_{>0}$ that is strictly decreasing and $\sigma(s) \to 0$ when $s \to \infty$. A function $\beta : \mathbb{R}_{\geq 0} \times \mathbb{R}_{\geq 0} \to \mathbb{R}_{\geq 0}$ is said to be of class $\mathcal{KL}$ if $\beta(\cdot, t) \in \mathcal{K}$ for all $t \in \mathbb{R}_{\geq 0}$ and $\beta(s, \cdot) \in \mathcal{L}$ for all $s \in \mathbb{R}_{\geq 0}$. A closed ball of radius δ centered at the origin is denoted by $\mathcal{B}_\delta := \{x \in \mathbb{R}^n \ : \ |x| \leq \delta\}$ where $|\cdot|$ is the Euclidean norm, and its interior is denoted $\mathring{\mathcal{B}}_\delta$. We define $|x|_\delta := \inf_{z \in \mathcal{B}_\delta} |x - z|$, and the subset $H(\delta, \Delta) := \{x \in \mathbb{R}^n \mid \delta \leq |x| \leq \Delta\}$. The definitions for UAS of a ball used in this paper are the same as presented in [18], and are restated here for completeness. Consider a system

$$\dot{x} = f(t, x), \tag{1}$$

where $x \in \mathbb{R}^n$, $t \in \mathbb{R}_{\geq 0}$ and $f : \mathbb{R}_{\geq 0} \times \mathbb{R}^n \to \mathbb{R}^n$ is continuous in t, and Lipschitz in x. Additionally, we define δ and Δ as nonnegative numbers such that $\Delta > \delta$.

Definition 1: (Uniform stability of a ball) The ball $\mathcal{B}_\delta$ is said to be uniformly stable on $\mathcal{B}_\Delta$ for system (1) if there exists a class $\mathcal{K}_\infty$ function α such that the solutions of (1) from any initial state $x_0 \in \mathbb{B}_\Delta$ and any initial time $t_0 \in \mathbb{R}_{\geq 0}$ satisfy $|x(t, t_0, x_0)|_\delta \leq \alpha(|x_0|)$ for all $t \geq t_0$.

Definition 2: (Uniform attractiveness of a ball) The ball $\mathcal{B}_\delta$ is said to be uniformly attractive on $\mathcal{B}_\Delta$ for system (1) if there exists a class $\mathcal{L}$ function σ such that the solutions of (1) from any initial state $x_0 \in \mathcal{B}_\Delta$ and initial time $t_0 \in \mathbb{R}_{\geq 0}$ satisfy $|x(t, t_0, x_0)|_\delta \leq \sigma(t - t_0)$ for all $t \geq t_0$.

Definition 3: (UAS of a ball) The ball $\mathcal{B}_\delta$ is said to be uniformly asymptotically stable on $\mathcal{B}_\Delta$ for the system (1) if it is both uniformly attractive and uniformly stable on $\mathcal{B}_\Delta$.

III. Uniform Practical Asymptotic Stability

In this section we provide Lyapunov sufficient conditions for UPAS of a time-varying nonlinear system, and we present results on the stability of cascaded systems consisting of UPAS sub-systems.

A. UPAS Definition

The definition of UPAS is presented in [19] and is restated here for completeness. We consider parameterized time-varying dynamical systems on the following form:

$$\dot{x} = f(t, x, \theta), \tag{2}$$

where $x \in \mathbb{R}^n$, $t \in \mathbb{R}_{\geq 0}$, $\theta \in \mathbb{R}^m$ is a constant parameter, typically a control gain that can be tuned and $f : \mathbb{R}_{\geq 0} \times \mathbb{R}^n \times \mathbb{R}^m \to \mathbb{R}^n$ is locally Lipschitz in x and piece-wise continuous in t and θ.

Definition 4: (UPAS) Let $\Theta \subset \mathbb{R}^m$ be a set of parameters. The system (2) is said to be Uniformly Practically Asymptotically Stable (UPAS) on Θ if for some $\Delta > 0$, for any positive $\delta < \Delta$ there exists $\theta^*(\delta) \in \Theta$ such that the ball $\mathcal{B}_\delta$ is UAS on $\mathcal{B}_\Delta$ for the system (2).

Note that this is a local adaptation of UGPAS and USPAS as presented in [16] and [18]. Specifically, if the radius Δ of $\mathcal{B}_\Delta$ can be increased arbitrarily by the choice of parameters, the definition extends to that of USPAS, and if $\Delta \to \infty$ regardless of the parameters selected, then it becomes the definition of UGPAS. The set of parameters for which the UPAS property holds is defined as $D_f(a, b) := \{\theta \in \mathbb{R}^m \mid \mathcal{B}_a \text{ is UAS on } \mathcal{B}_b \text{ for (2)}\}$.

B. Lyapunov Sufficient Conditions for UPAS

The following theorem is an adaptation of Theorem 10 in [18] and gives sufficient conditions for a system on the form (2) to be UPAS.

Theorem 1: (Lyapunov sufficient conditions for UPAS) Suppose that there exists a $\Delta > 0$ such that, for any positive $\delta < \Delta$ there exist a parameter $\theta^*(\delta) \in \Theta$, a continuously differentiable function $V_\delta : \mathbb{R}_{\geq 0} \times \mathbb{R}^n \to \mathbb{R}_{\geq 0}$, and class $\mathcal{K}$-functions $\underline{\alpha}_\delta$, $\overline{\alpha}_\delta$ and α_δ, such that for all $x \in H(\delta, \Delta)$, and all $t \in \mathbb{R}_{\geq 0}$

$$\underline{\alpha}_\delta(|x|) \leq V_\delta(t, x) \leq \overline{\alpha}_\delta(|x|), \tag{3}$$

$$\frac{\partial V_\delta}{\partial t}(t, x) + \frac{\partial V_\delta}{\partial x}(t, x) f(t, x, \theta^*) \leq -\alpha_\delta(|x|), \tag{4}$$

$$\lim_{\delta \to 0} \underline{\alpha}_\delta^{-1} \circ \overline{\alpha}_\delta(\delta) = 0. \tag{5}$$

then the system (2) is UPAS on the parameter set Θ.

The proof of Theorem 1 is given in Appendix B. It is worth stressing that the $\mathcal{K}$ functions involved in (3) - (4) typically depend on the the value of the parameter θ, which is itself tuned to reach a given steady-state precision δ. In other words, these $\mathcal{K}$ functions typically depend on δ, as indicated by the subscript. This is what makes condition (5) nontrivial.

The conditions stated in Theorem 1 are similar to those given in [19, Corollary 2], but differ in how the bounds (3), which V has to satisfy, are defined. In [19, Corollary 2] the bounds are given in terms of powers of the norm of the state, in particular the same power for both the lower and upper bound, and the bounds also depend on a set of functions of the system parameters. Here the bounds are given in terms of arbitrary class $\mathcal{K}$ functions which depend on δ instead of the parameter θ.

C. UPAS of Cascades

We consider the cascaded system

$$\dot{x}_1 = f_1(t, x_1, \theta_1) + g(t, x, \theta) x_2, \tag{6a}$$

$$\dot{x}_2 = f_2(t, x_2, \theta_2), \tag{6b}$$

where $x := [x_1^T, x_2^T]^T \in \mathbb{R}^{n_1} \times \mathbb{R}^{n_2}$ are the states, $\theta := [\theta_1^T, \theta_2^T]^T \in \mathbb{R}^{m_1} \times \mathbb{R}^{m_2}$ are the parameters, $t \in \mathbb{R}_{\geq 0}$, f_1, f_2 and g are locally Lipschitz in the states and parameters, and piece-wise continuous in time. The subsystems (6a) and (6b) are the driven and driving subsystem, respectively, and $\dot{x}_1 = f_1(t, x_1, \theta_1)$ will be referred to as the nominal dynamics of the driven subsystem. Additionally, we make the assumption

Assumption 1: (Boundedness of the interconnection term) The function g is uniformly bounded both in time and parameters, i.e there exists a nondecreasing function $G : \mathbb{R}_{\geq 0} \to \mathbb{R}_{\geq 0}$ such that, for all $x \in \mathbb{R}^{n_1} \times \mathbb{R}^{n_2}$, all $\theta \in \Theta_1 \times \Theta_2$ and all $t \in \mathbb{R}_{\geq 0}$

$$|g(t, x, \theta)| \leq G(|x|). \tag{7}$$

To establish UPAS of cascaded systems on the form given by (6), an adaptation of Theorem 13 in [18] is made. The following assumptions are made:

Assumption 2: (UPAS of the driving subsystem) The driving system (6b) is UPAS on Θ_2.

Assumption 3: (UPAS of the driven subsystem) For some $\Delta_1 > 0$ and any δ_1 such that $\Delta_1 > \delta_1 > 0$, there exist a parameter $\theta_1^*(\delta_1) \in \Theta_1$, a continuously differentiable function V_{δ_1}, and class $\mathcal{K}$ functions $\underline{\alpha}_{\delta_1}$, $\overline{\alpha}_{\delta_1}$ and α_{δ_1} such that conditions (3), (4) and (5) are satisfied with these functions, and a continuous positive nondecreasing function c_{δ_1} exists such that for all $x_1 \in H(\delta_1, \Delta_1)$ and all $t \in \mathbb{R}_{\geq 0}$

$$\left| \frac{\partial V_{\delta_1}}{\partial x_1}(t, x_1) \right| \leq c_{\delta_1}(|x_1|). \tag{8}$$

In [20], we also assumed that solutions of (6) starting sufficiently close to the origin are bounded. However, it can be shown that boundedness of solutions follows from Assumptions 2-1. We summarize this in the following proposition:

Proposition 1: (Boundedness of solutions) Given Assumptions 1-3, then there exist positive constants Δ_0, δ_1, δ_2, γ such that the trajectories of (6) with $\theta = \theta^*$, where $\theta_1^*(\delta_1) \in \Theta_1$ is given by Assumption 3 and $\theta_2^* \in D_{f_2}(\delta_2, \Delta_2) \cap \Theta_2$, satisfy

$$|x_0| \leq \gamma \;\Rightarrow\; |x(t, t_0, x_0, \theta^*)| < \Delta_0, \; \forall t \geq t_0 \tag{9}$$

The proof of Proposition 1 is given in Appendix B. It is worth noting that the proof only requires $|x_2(t)|_{\delta_2}$ to be bounded by a class $\mathcal{K}$ function, not class $\mathcal{KL}$. As a consequence, the conditions of Proposition 1 could be relaxed for the driving subsystem, requiring only that there is a ball $\mathcal{B}_{\delta_2}$ which is US on some $\mathcal{B}_{\Delta_2}$. With Proposition 1, we can now restate the theorem from [20] with fewer conditions:

Theorem 2: Under Assumptions 1-3 the cascaded system (6) is UPAS on $\Theta_1 \times \Theta_2$.

The proof of Theorem 2 is given in Appendix C.

IV. Control-Oriented Model

A detailed model of a USR, where the full kinematics and dynamics of a planar snake robot with revolute joints are considered, is presented in [21]. The complexity of this model makes it less appropriate for the design of control systems and motion planning. A simplified control-oriented model was thus developed for terrestrial snake robots in [22]. It was extended to include hydrodynamic effects for USRs in [23], and developed further in [24], where constant ocean currents

were added. In the control-oriented model it is assumed that during undulatory motion the motion of the angular joints can be approximated by prismatic joints, where all joints point in the heading direction of the USR, as illustrated in Fig. 1. In this paper we allow the component of the current along the y-axis to be time-varying. The control-oriented model is then given by:

$$\dot{\boldsymbol{\phi}} = \boldsymbol{v}_\phi, \tag{10a}$$
$$\dot{\eta} = r, \tag{10b}$$
$$\dot{p}_x = v_t \cos\eta - v_n \sin\eta + V_x, \tag{10c}$$
$$\dot{p}_y = v_t \sin\eta + v_n \cos\eta + V_y(t), \tag{10d}$$
$$\dot{\boldsymbol{v}}_\phi = -\frac{c_n}{m}\boldsymbol{v}_\phi + \frac{c_p}{m} v_t \boldsymbol{A}\boldsymbol{D}^T\boldsymbol{\phi} + \frac{1}{m}\boldsymbol{D}\boldsymbol{D}^T\boldsymbol{u}, \tag{10e}$$
$$\dot{r} = -\lambda_1 r + \frac{\lambda_2}{N_l - 1} v_t \bar{\boldsymbol{e}}^T\boldsymbol{\phi}, \tag{10f}$$
$$\dot{v}_t = -\frac{c_t}{m}v_t + \frac{2c_p}{N_l m}\bar{\boldsymbol{e}}^T\boldsymbol{\phi} v_n - \frac{c_p}{N_l m}\boldsymbol{\phi}^T\boldsymbol{A}\bar{\boldsymbol{D}}\boldsymbol{v}_\phi + r(V_x \sin\eta - V_y(t)\cos\eta) - \dot{V}_y(t)\sin\eta, \tag{10g}$$
$$\dot{v}_n = -\frac{c_n}{m}v_n + \frac{2c_p}{N_l m}\bar{\boldsymbol{e}}^T\boldsymbol{\phi} v_t + r(V_x \cos\eta + V_y(t)\sin\eta) - \dot{V}_y(t)\cos\eta. \tag{10h}$$

Here $\boldsymbol{\phi}$ contains all the relative $N_l - 1$ joint angles ϕ_i while η denotes the heading of the snake robot. The position of the USR is given by $[p_x, p_y]^T$. The angular velocity of the joints is given by $\boldsymbol{v}_\phi$, while the angular velocity of the heading is given by r. The velocities relative to the ocean current are given by v_t and v_n, respectively. Additionally, current velocity is given by $[V_x, V_y(t)]^T$, where $V_y(t)$ is time-varying and bounded. Additionally we define $|V_\alpha|$ to be the upper bound of the magnitude of $V_y(t)$. Furthermore, $\lambda_i > 0$ are constants that characterize the rotational dynamics. The coeffcients $c_t > 0, c_n > 0$ are the drag coefficients in the tangential and normal directions, respectively, while $c_p > 0$ is the propulsion coefficient. The actuation torque from the motorized joints is given by $\boldsymbol{u}$. The summation vector is denoted as $\bar{\boldsymbol{e}} = [1, \ldots, 1]^T \in \mathbb{R}^{N_l - 1}$, and the matrix $\bar{\boldsymbol{D}} = \boldsymbol{D}^T(\boldsymbol{D}\boldsymbol{D}^T)^{-1}$. The $\boldsymbol{A}$ and $\boldsymbol{D}$ are given by $\boldsymbol{D} = \begin{bmatrix} 1 & -1 & & \\ & \ddots & \ddots & \\ & & 1 & -1 \end{bmatrix}$, $\boldsymbol{A} = \begin{bmatrix} 1 & 1 & & \\ & \ddots & \ddots & \\ & & 1 & 1 \end{bmatrix}$.

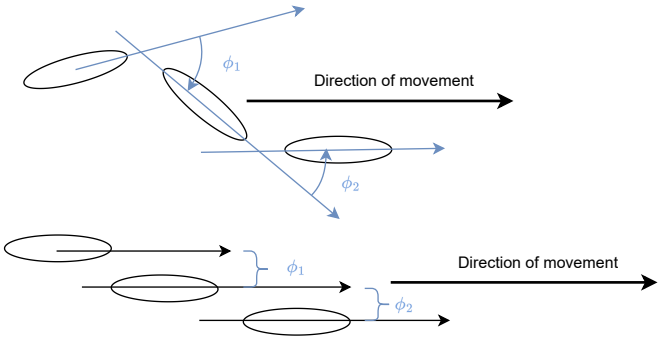

Fig. 1: Illustration of the transformation between the complex model at the top, and the control-oriented model, at the bottom.

V. Control Design

A. Control Objectives and Approach

The approach presented in this paper is inspired by [9], [10], [13], and developed for the control-oriented model presented in Section IV. However, because the proposed controller is designed to handle time-varying references and disturbances, the hierarchical approach as used in these papers, can not be used in our control design and analysis. Moreover, both the attitude and the initial position require restrictions of initial states to converge to their desired values. Therefore, theory for global or semiglobal stability properties will not be applicable, and we instead show local properties. Furthermore, the time-varying current introduces nonvanishing perturbations, which in turn lead to solutions converging towards a vicinity around the origin. Therefore, a cascaded system approach based on the results of Section III is utilized.

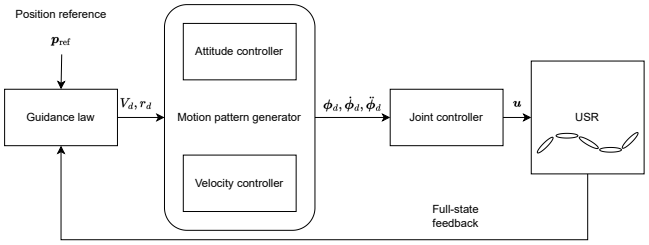

Fig. 2: Block diagram of control system.

The control objective is to stabilize the position close to the desired position

$$\limsup_{t\to\infty} |e_x(t)| \leq \delta_x, \limsup_{t\to\infty} |e_y(t)| \leq \delta_y, \tag{11}$$

where, e_x and e_y represent horizontal and vertical position error variables, respectively, with corresponding errors from the desired position denoted as δ_x and δ_y, which can be arbitrarily diminished by choice of system parameters. To achieve this, each link's joint angle ϕ_i is controlled to follow a sinusoidal gait, which has been shown to induce forward motion in [25]. The sinusoidal gait is given by

$$\phi_{d,i} = \alpha\gamma_1(i)\sin(\lambda + (i-1)\delta) + g_2(\phi_0), \tag{12}$$

where α is the amplitude, $\gamma_1(i)$ is a scaling function that varies the amplitude along the snake body, and δ is the phase shift between adjacent joints. The frequency and turning parameters are the variables λ and ϕ_0. A saturation function g_2 is designed to be strictly increasing and twice differentiable in the range $[\phi_{0,\min}, \phi_{0,\max}]$. The control system is illustrated in Fig. 2. The guidance law generates a reference tangential velocity V_d and angular velocity r_d, driving the USR towards the desired position. The motion pattern generator then generates the sinusoidal gait pattern, where the gait frequency is used to control the velocity, and the turning parameter is used to control the angular velocity to achieve the references given by the guidance law. Finally, the joint controller calculates the input torque u_i for each joint to follow the desired sinusoidal pattern. The inputs and reference joint angles are assembled into the vectors $\boldsymbol{u} \in \mathbb{R}^{N_l - 1}$ and $\boldsymbol{\phi}_d \in \mathbb{R}^{N_l - 1}$, respectively. To

drive the joint angles to the desired values, the time derivatives $\dot{\boldsymbol{\phi}}_d$ and $\ddot{\boldsymbol{\phi}}_d$ are needed, as will be shown in Section V-B. Therefore, it is natural to use the second derivatives of the gait frequency and turning parameters as virtual inputs when designing the velocity and attitude controllers, $\ddot{\lambda} = u_\lambda$ and $\ddot{\phi}_0 = u_\phi$.

B. Joint Controller

To achieve the desired relative angles, the following feedback linearizing controller is proposed

$$\boldsymbol{u} = m(\boldsymbol{D}\boldsymbol{D}^T)^{-1}[\frac{c_n}{m}\boldsymbol{v}_\phi - \frac{c_p}{m}v_t\boldsymbol{A}\boldsymbol{D}^T\dot{\boldsymbol{\phi}} + \bar{\boldsymbol{u}}]. \tag{13}$$

We choose $\bar{\boldsymbol{u}} = \ddot{\boldsymbol{\phi}}_d - K_{\phi,1}\dot{\tilde{\boldsymbol{\phi}}} - K_{\phi,2}\tilde{\boldsymbol{\phi}}$, where $K_{\phi,1}$, $K_{\phi,2} > 0$, and $\tilde{\boldsymbol{\phi}} = \boldsymbol{\phi} - \boldsymbol{\phi}_d$. Inserting (13) into (10e) yields

$$\ddot{\tilde{\boldsymbol{\phi}}} + K_{\phi,1}\dot{\tilde{\boldsymbol{\phi}}} + K_{\phi,2}\tilde{\boldsymbol{\phi}} = 0, \tag{14}$$

We can then state the following proposition, which will be used in the analysis of the complete system through Propositions 3-7.

Proposition 2: The origin of the system (14) is uniformly globally exponentially stable (UGES).

Proof: Since $K_{\phi,1}$ and $K_{\phi,2}$ are positive definite matrices, the system (14) is a linear time-invariant system with negative eigenvalues, and thus the origin is UGES. ■

C. Velocity Controller

The objective of the velocity controller is to adjust the frequency of the sinusoidal gait (12) so that $\lim_{t\to\infty} v_t = V_d$. The control input u_λ appears in the second derivative of the relative tangential velocity dynamics. Therefore, we employ an integrator backstepping approach to design the velocity controller. We define the error variables $z_1 := v_t - V_d$ and $z_2 := \dot{\lambda} - \zeta_1$, where ζ_1 is a virtual control input, which is used to stabilize z_1. The error dynamics are derived by considering (10g) and (12), and defining $\psi_1(\cdot)$ such that

$$\begin{aligned}\dot{z}_1 = &-\frac{c_t}{m}v_t + \psi_1(t, v_n, v_\theta, \eta) - X_\phi\dot{\phi}_0 \\ &- X_\lambda(\zeta_1 + z_2) + g_1(\tilde{\boldsymbol{\phi}}, \dot{\tilde{\boldsymbol{\phi}}}),\end{aligned} \tag{15}$$

where we define $\bar{\boldsymbol{B}} := \boldsymbol{A}\bar{\boldsymbol{D}}$ and

$$g_1(t, \tilde{\boldsymbol{\phi}}, \dot{\tilde{\boldsymbol{\phi}}}) := -\frac{c_p((2\tilde{\boldsymbol{\phi}} + \boldsymbol{\phi}_d)^T\bar{\boldsymbol{B}}\dot{\tilde{\boldsymbol{\phi}}} + \dot{\tilde{\boldsymbol{\phi}}}^T\bar{\boldsymbol{B}}\dot{\boldsymbol{\phi}}_d)}{N_l m}, \tag{16a}$$

$$X_\phi := \frac{c_p}{N_l m}\boldsymbol{\phi}_d^T\bar{\boldsymbol{B}}, \tag{16b}$$

$$X_\lambda := X_\phi\alpha[\cos(\lambda) + ... + \cos(\lambda + \delta(N_l - 1))]. \tag{16c}$$

We choose the virtual control input as

$$\zeta_1 = \frac{-\frac{c_t}{m}V_d - \psi_1(t, v_n, v_\theta, \eta) - X_\phi\dot{\phi}_0 + K_{\lambda,1}z_1}{X_\lambda}, \tag{17a}$$

$$\zeta_1 = \frac{\zeta_1^* - X_\phi\dot{\phi}_0}{X_\lambda}. \tag{17b}$$

The derivative of the second error variable z_2 is the found as

$$\dot{z}_2 = u_\lambda - \frac{\dot{\zeta}_1^*}{X_\lambda} + \frac{\dot{X}_\lambda(\zeta_1^* + X_\phi\dot{\phi}_0)}{X_\lambda^2} - \frac{X_\phi\ddot{\phi}_0 + \dot{X}_\phi\dot{\phi}_0}{X_\lambda}. \tag{18}$$

The control input is then selected as

$$u_\lambda = \frac{\dot{\zeta}_1^* + \dot{X}_\phi\dot{\phi}_0}{X_\lambda} - \frac{\dot{X}_\lambda(\zeta_1^* + X_\phi\dot{\phi}_0)}{X_\lambda^2} - K_{\lambda,2}z_2 + X_\lambda z_1. \tag{19}$$

By inserting the virtual input (17) and the control input (19), the closed-loop system is then given by

$$\dot{z}_1 = -\left(\frac{c_t}{m} + K_{\lambda,1}\right)z_1 - X_\lambda z_2 + g_1(t, \tilde{\phi}, \dot{\tilde{\phi}}), \tag{20a}$$

$$\dot{z}_2 = -K_{\lambda,2}z_2 + X_\lambda z_1 + \frac{X_\phi}{X_\lambda}u_\phi. \tag{20b}$$

We define the parameter set $\boldsymbol{\varphi}_1 := [\boldsymbol{\varphi}_2, \boldsymbol{\varphi}_3]^T$, where $\boldsymbol{\varphi}_2 := [K_{\phi,1}, K_{\phi,2}]^T$ and $\boldsymbol{\varphi}_3 := [K_{\lambda,1}, K_{\lambda,2}]^T$, and state variables $\boldsymbol{x}_1 := [z_1, z_2]^T$ and $\boldsymbol{x}_2 := [\tilde{\boldsymbol{\phi}}, \dot{\tilde{\boldsymbol{\phi}}}]^T$. The cascaded system can then be written as

$$\dot{\boldsymbol{x}}_1 = \boldsymbol{f}_1(t, \boldsymbol{x}_1, \boldsymbol{x}_2, \boldsymbol{\varphi}_2) + \boldsymbol{g}_\lambda(t, \boldsymbol{x}_2)\boldsymbol{x}_2, \tag{21a}$$

$$\dot{\boldsymbol{x}}_2 = \boldsymbol{f}_2(\boldsymbol{x}_2, \boldsymbol{\varphi}_3), \tag{21b}$$

where the dynamics and interconnection-term are given by (14), (20) and (16a).

Proposition 3: The cascaded system (21), with the backstepping controller (19) is UPAS on $\boldsymbol{\varphi}_1$ and the solutions are globally uniformly bounded (GUB).

Proof: Consider the Lyapunov function defined as $V_1 := (1/2)z_1^2 + (1/2)z_2^2$. From Proposition 2 it is known that $\boldsymbol{x}_2$ is bounded. Furthermore, the references $\boldsymbol{\phi}_d$ and $\dot{\boldsymbol{\phi}}_d$ are bounded by design. This implies that g_1, X_ϕ and X_λ are bounded. We denote the bounds by $g_{1,m}$, $X_{\phi,m}$ and $X_{\lambda,m}$. The following bound of the Lie derivative is then derived:

$$\begin{aligned}\dot{V}_1 \leq &-\left[\left(\frac{c_t}{m} + K_{\lambda,1}\right)|z_1| - g_{1,m}\right]|z_1| \\ &-\left(K_{\lambda,2}|z_2| - \frac{X_{\phi,m}}{X_{\lambda,m}}u_{\phi,m}\right)|z_2|,\end{aligned} \tag{22}$$

where $u_{\phi,m}$ is the bound of the angular velocity control input. The derivative (22) is negative definite for

$$|\boldsymbol{x}_1| > \frac{g_{1,m}}{\frac{c_t}{m} + K_{\lambda,1}} + \frac{X_{\phi,m}}{X_{\lambda,m}K_{\lambda,2}}|u_{\phi,m}|. \tag{23}$$

This means that $\boldsymbol{x}_1$ is GUB by Theorem 4.18 in [26]. From the choice of V_1 and (22) it follows that the driven subsystem satisfies Assumption 3, and the interconnection term is bounded.

Finally it is established in Proposition 2 that the driving system is UGES. Then by Theorem 2 the system is UPAS on the set of parameters. ■

D. Guidance Law and Attitude Controller

The guidance law presented in this paper is inspired by [11]–[13]. The planar geometric path following guidance law is modified to include a desired velocity u_y along the y-axis in addition to the velocity u_x along the x-axis. The velocity references will be designed to stabilize the position of the USR in Section V-E. The goal of the attitude controller is to achieve a desired orientation that drives the USR toward the desired

position, using u_{ϕ_0} as input. The desired orientation is defined as

$$\boldsymbol{R_d} := \begin{bmatrix} \frac{u_x - V_x}{V_d} & \frac{u_y}{V_d} \\ -\frac{u_y}{V_d} & \frac{u_x - V_x}{V_d} \end{bmatrix}, \tag{24}$$

where $V_d = \sqrt{(u_x - V_x)^2 + (u_y)^2}$. This is illustrated in Figure 3 below. We define the error function $\Psi(\boldsymbol{R}, \boldsymbol{R_d})$ as

$$\Psi(\boldsymbol{R}, \boldsymbol{R_d}) := \frac{1}{2}\text{tr}[I - \boldsymbol{R_d}^T \boldsymbol{R}]. \tag{25}$$

Furthermore, the derivative of $\Psi(\cdot)$ with respect to $\boldsymbol{R}$ is defined as $\boldsymbol{D}_R\Psi(\boldsymbol{R}, \boldsymbol{R_d}) := e_R$, where e_R is given by

$$\begin{bmatrix} 0 & -e_R \\ e_R & 0 \end{bmatrix} = \frac{1}{2}(\boldsymbol{R_d}^T \boldsymbol{R} - \boldsymbol{R}^T \boldsymbol{R_d}). \tag{26}$$

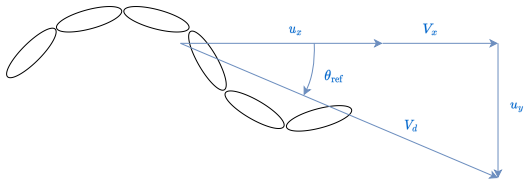

Fig. 3: Geometric representation of guidance law.

As in [13], the desired angular velocity is found to be

$$\begin{bmatrix} 0 & -r_d \\ r_d & 0 \end{bmatrix} = \boldsymbol{R_d}^T \dot{\boldsymbol{R}}_{\boldsymbol{d}}. \tag{27}$$

By defining $y_1 := r - r_d$ and the choice of r_d given by (27) the following can be found

$$\frac{d\Psi(\boldsymbol{R}, \boldsymbol{R_d})}{dt} = e_R y_1, \tag{28a}$$

$$\dot{e}_R = C y_1, \tag{28b}$$

where $|C| \leq 1$. The error function $\Psi(\boldsymbol{R}, \boldsymbol{R_d}) \in [0, 2]$, where $\Psi(\boldsymbol{R}, \boldsymbol{R_d}) = 0$ implies that the heading of the USR is aligned with the desired orientation, while $\Psi(\boldsymbol{R}, \boldsymbol{R_d}) = 2$ implies that the USR is pointed in the opposite direction of the desired orientation. From (26) we see that $e_R = 0$ when $\boldsymbol{R} = \boldsymbol{R_d}$ and $\boldsymbol{R} = -\boldsymbol{R_d}$, implying that there are two equilibrium points in the dynamics of the orientation.

Motivated by [12], [13] we define the subset level $L_2 := \{\boldsymbol{R} \in SO(2) | \Psi(\boldsymbol{R}, \boldsymbol{R}_d) < 2\}$. The attitude controller is designed to ensure that given some initial conditions, $\boldsymbol{R}$ always lies in L_2. The error dynamics are defined as $y_2 := g_2(\phi_0) - \chi_1$, $y_3 := \dot{\phi}_0 - \chi_2$, where χ_1 and χ_2 are virtual inputs.

We define the interconnection term and sinusoidal gait signals

$$g_3(t, \tilde{\boldsymbol{\phi}}, z_1) := \frac{\lambda_2}{N_l - 1}((z_1 + V_d)\bar{\boldsymbol{e}}^T \tilde{\boldsymbol{\phi}} + z_1 \bar{\boldsymbol{e}}^T \boldsymbol{\phi}_d), \tag{29a}$$

$$\alpha_1(\lambda) := \alpha[\sin(\lambda), ..., \sin(\lambda + \delta(N_l - 1))]^T. \tag{29b}$$

The virtual inputs are then selected as

$$\chi_1 = \frac{\lambda_1 r_d - \lambda_2 V_d \alpha(\lambda) - \dot{r}_d - K_1 z_1 - K_R e_R}{\lambda_2 V_d}, \tag{30a}$$

$$\chi_2 = \frac{1}{\partial g(\phi_0)/\partial \phi_0}\left[\dot{\chi}_1 - \lambda_2 V_d y_1 - K_2 y_2\right], \tag{30b}$$

$$u_\phi = \dot{\chi}_2 - \frac{\partial g(\phi_0)}{\partial \phi_0} y_2 - K_3 y_3. \tag{30c}$$

This gives the following closed loop dynamics

$$\begin{aligned} \dot{y}_1 = &-(\lambda_1 + K_1) y_1 + \lambda_2 V_d y_2 \\ &- K_R e_R + g_3(t, \tilde{\boldsymbol{\phi}}, z_1), \end{aligned} \tag{31a}$$

$$\dot{y}_2 = \frac{\partial g_2(\phi_0)}{\partial \phi_0} y_3 - \lambda_2 V_d y_1 - K_2 y_2, \tag{31b}$$

$$\dot{y}_3 = -\frac{\partial g_2(\phi_0)}{\partial \phi_0} y_2 - K_3 y_3. \tag{31c}$$

We define $\boldsymbol{x}_3 := [e_R, y_1, y_2, y_3]^T$, $\boldsymbol{x}_4 := [\boldsymbol{x}_1, \boldsymbol{x}_2]^T$, $\boldsymbol{\varphi}_4 := [K_1, K_2, K_3, K_R]^T$, $\boldsymbol{\varphi}_5 := [\boldsymbol{\varphi}_4, \boldsymbol{\varphi}_1]^T$ and the initial states y_{i0}. We then have the following cascaded system

$$\dot{\boldsymbol{x}}_3 = \boldsymbol{f}_3(t, \boldsymbol{x}_3, \boldsymbol{\varphi}_4) + \boldsymbol{g}_3(t, \boldsymbol{x}_4), \tag{32a}$$

$$\dot{\boldsymbol{x}}_4 = \boldsymbol{f}_4(t, \boldsymbol{x}_4, \boldsymbol{\varphi}_1), \tag{32b}$$

where $\boldsymbol{f}_3$, $\boldsymbol{g}_3$ and $\boldsymbol{f}_4$ are given by (31), (28) and (21). The following proposition can then be made:

Proposition 4: Consider a system with dynamics (10) and controller (30), and suppose that the initial conditions satisfy

$$\Psi(\boldsymbol{R}(0), \boldsymbol{R}_d(0)) < 2, \tag{33a}$$

$$y_{10}^2 + y_{20}^2 + y_{30}^2 < 2K_R(2 - \Psi(\boldsymbol{R}(0), \boldsymbol{R}_d(0))). \tag{33b}$$

Then, for sufficiently small values of $\tilde{\boldsymbol{\phi}}$ and z_1, and by selecting K_1 such that

$$\frac{g_{3,m}}{(\lambda_1 + K_1)} << 2K_R \tag{34}$$

it can be shown that $\Psi(\boldsymbol{R}(0), \boldsymbol{R}_d(0)) \in L_2$ $\forall t$.

Proof: We define $V_2 := \frac{1}{2}y_1^2 + \frac{1}{2}y_2^2 + \frac{1}{2}y_3^2 + K_R\Psi(\boldsymbol{R}, \boldsymbol{R_d})$. To ensure that $\Psi(\boldsymbol{R}(t), \boldsymbol{R}_d(t)) < 2$ the derivative of V_2 has to be negative definite when approaching the ball β_r where $r = 2K_R$. From Proposition 3 it follows that z_1 is bounded. Furthermore V_d is bounded by design. We define $g_{3,m}$ and V_m as the bound of the interconnection term and desired relative tangential velocity, respectively. Then the following bound is found for the derivative of the Lyapunov function

$$\begin{aligned} \dot{V}_2 \leq &-(\lambda_1 + K_1)|y_1|^2 - K_2|y_2|^2 - K_3|y_3|^2 \\ &+ g_{3,m}|y_1|. \end{aligned} \tag{35}$$

By selecting the gains as in (34), the Lyapunov function is negative definite when approaching a circle with radius $2K_R$, implying that if the initial values satisfy (33) the states are bounded away from β_r $\forall t$. ■

We now state a proposition for the cascaded system (32) to be UPAS. Let $\lambda_m(\boldsymbol{A})$ and $\lambda_M(\boldsymbol{A})$ denote the largest and smallest eigenvalues for a square matrix $\boldsymbol{A}$.

Proposition 5: Consider a system with dynamics (10) and the controller given by (30) and assume that the bounds given by (34) are satisfied and that

$$K_2 > \frac{\lambda_2 V_m}{2,} \tag{36a}$$

$$\lambda_m(\boldsymbol{M}_{3,\phi}) > \frac{\lambda_2 V_m}{2}. \tag{36b}$$

Then (32a) is UAS and the cascaded system given by (32) is UPAS on $\boldsymbol{\varphi}_5$.

Proof: To show stability for the attitude dynamics, the following bounds are used

$$\frac{1}{2}||e_R||^2 \leq \Psi(\boldsymbol{R}, \boldsymbol{R}_d) \leq \frac{1}{2-\psi_\phi}||e_R||^2, \tag{37}$$

where $\Psi(\boldsymbol{R}, \boldsymbol{R}_d) \leq \psi_\phi < 2$, which is derived and proven in [12]. A new Lyapunov function is defined as $V_3 := V_2 + \frac{1}{2}\beta_\phi e_R y_1$, where β_ϕ is a positive constant. By using the bounds (37), it can be shown that the Lyapunov function is bounded by

$$\boldsymbol{x}_3^T \boldsymbol{M}_{\phi,1} \boldsymbol{x}_3 \leq V_3 \leq \boldsymbol{x}_3^T \boldsymbol{M}_{\phi,2} \boldsymbol{x}_3, \tag{38}$$

where

$$\boldsymbol{M}_{\phi,1} = \frac{1}{2}\begin{bmatrix} K_R & -\beta_\phi & 0 & 0 \\ -\beta_\phi & 1 & 0 & 0 \\ 0 & 0 & 1 & 0 \\ 0 & 0 & 0 & 1 \end{bmatrix}, \boldsymbol{M}_{\phi,2} = \frac{1}{2}\begin{bmatrix} \frac{2K_R}{2-\psi_\phi} & \beta_\phi & 0 & 0 \\ \beta_\phi & 1 & 0 & 0 \\ 0 & 0 & 1 & 0 \\ 0 & 0 & 0 & 1 \end{bmatrix}. \tag{39}$$

Selecting $\beta_\phi < \sqrt{K_R}$, the eigenvalues of $\boldsymbol{M}_{\phi,1}$ and $\boldsymbol{M}_{\phi,2}$ are positive, and the following bounds can be used

$$\lambda_m(\boldsymbol{M}_{\phi,1})||\boldsymbol{x}_3||^2 \leq V_3 \leq \lambda_M(\boldsymbol{M}_{\phi,2})||\boldsymbol{x}_3||^2, \tag{40}$$

We consider the nominal part of the dynamics (31), and find the following bound for $\dot{V}_3$

$$\begin{aligned} \dot{V}_3 \leq -\boldsymbol{x}_5^T \begin{bmatrix} \beta_\phi K_R & -\frac{\beta_\phi(\lambda_1+K_1)}{2} \\ -\frac{\beta_\phi(\lambda_1+K_1)}{2} & ((\lambda_1+K_1)-\beta_\phi) \end{bmatrix} \boldsymbol{x}_5 \\ - K_2 y_2^2 - K_3 y_3^2 + \lambda_2 V_d y_2 e_R, \end{aligned} \tag{41}$$

where $\boldsymbol{x}_5 = [\,|e_R| \;\; |y_1|\,]^T$. By selecting

$$\beta_\phi < \min\left\{(\lambda_1 - K_1), \frac{4K_R(\lambda_1+K_1)}{4K_R + (\lambda_1+K_1)^2}, \sqrt{K_R}\right\}, \tag{42}$$

the matrix in (41), which we denote as $\boldsymbol{M}_{\phi,3}$, is positive definite. Using Young's inequality [27] the bound can be rewritten as

$$\begin{aligned} \dot{V}_3 \leq -\lambda_m(\boldsymbol{M}_{\phi,3})|y_1|^2 - (K_2 - \frac{\lambda_2 V_d}{2})y_2^2 \\ - K_3 y_3^2 - (\lambda_m(\boldsymbol{M}_{\phi,3}) - \frac{\lambda_2 V_d}{2})|e_R|^2. \end{aligned} \tag{43}$$

The bound is negative definite if (36) are satisfied. This implies that the origin is UAS for the nominal dynamics of $\boldsymbol{x}_3$. Additionally all the conditions of Theorem 2 are satisfied and the cascaded system is UPAS on the set of parameters. ■

E. Position and Sway Velocity Stabilization

In this section, we show that the sway velocity is GUB, and that the position of the USR converges to some neighborhood around the origin. Motivated by [6], the point which defines the position of the robot is moved by a distance $\epsilon = -2(N-1)c_p/N_l m\lambda_2$. The new coordinates are given by

$$\dot{e}_x = v_t \cos\eta - \bar{v}_n \sin\eta + V_x, \tag{44a}$$

$$\dot{e}_y = v_t \sin\eta + \bar{v}_n \cos\eta + V_y(t), \tag{44b}$$

$$\dot{\bar{v}}_n = X(\eta)r - Y\bar{v}_n - \dot{V}_y(t)\cos\eta, \tag{44c}$$

where, $X(\eta) = \epsilon(c_n/m - \lambda_1) + V_x\cos\eta + V_y(t)\sin\eta$, and $Y = c_n/m$. We define $\boldsymbol{\varphi}_6 = [Y, \boldsymbol{\varphi}_5]^T$.

Proposition 6: Consider the USR described by (10), with the controllers (13), (19), (30) and the guidance law given in Section V-D. Then the transformed sway velocity $\bar{v}_n$ is GUB and the cascaded system is UPAS on $\boldsymbol{\varphi}_6$.

Proof: We consider (44c) and rewrite the equation to

$$\dot{\bar{v}}_n = X(\eta)r_d - Y\bar{v}_n + X(\eta)y_1 - \dot{V}_y(t)\cos\eta. \tag{45}$$

We define $V_4 := (1/2)\bar{v}_n^2$, and the derivative is bounded by

$$\dot{V}_4 \leq -Y\bar{v}_n^2 + (|V_\alpha| + |X_M|(|r_d| + |y_1|))|\bar{v}_n|, \tag{46}$$

where $X_M = (|X| + |V_x| + |V_\alpha|)$. By Proposition 5, y_1 is bounded. Furthermore r_d is bounded by design. We define the upper limit of $y_1 + r_d$ as r_M. By inserting this we get

$$\dot{V}_4 \leq -Y\bar{v}_n^2 + (|V_\alpha| + 2|X_M||r_M|)|\bar{v}_n|, \tag{47}$$

which is negative definite for $|\bar{v}_n| > (|V_\alpha| + 2|X_M||r_M|)/Y$ and therefore uniformly bounded by Theorem 4.18 in [26]. The nominal system is UPAS by Theorem 1, and V_4 satisfies the conditions of Assumption 3. The conditions of Theorem 2 are thus satisfied, and the cascaded system is UPAS on $\boldsymbol{\varphi}_6$. ■

To stabilize the position of the USR, it is necessary for the guidance law to be well defined, meaning that $V_d \neq 0$. The components u_x, u_y of the guidance law serve as control inputs for the position, and are selected as $u_x = -ke_x$ and $u_y = -ke_y$. Additionally it is assumed that $(-ke_x - V_x) > 0$, which implies that the USR always approaches the desired position from such a direction that the current component along the x-axis runs towards the USR.

Our goal is to design a controller that stabilizes the position of the USR at some desired position close to a bluff body. For efficient movement and energy harvesting purposes this would be downstream in the wake of an object. Therefore the assumption that the USR moves against the current is reasonable. We define $\tilde{\eta} := \eta - \eta_d$ and $\boldsymbol{\varphi}_7 = [k, \boldsymbol{\varphi}_6]^T$.

Proposition 7: Consider an USR described by (10), with the controllers (13), (19), (30) and the guidance law given in Section V-D. Furthermore, assume that the USR is moving against the current component along the x-axis, such that $(-ke_x - V_x) > 0$. Additionally, assume the attitude error $\tilde{\eta}$ is small and bounded such that it satisfies (48).

$$(1 - \frac{|\tilde{\eta}|^2}{2}) > 0. \tag{48}$$

Then the position errors $|e_x|$ and $|e_y|$ are GUB and the cascaded system is UPAS on $\boldsymbol{\varphi}_7$.

Proof:

$$|\dot{V}_5| \leq -k\left(1-\frac{\tilde{\eta}^2}{2}\right)(|e_y|^2+|e_x|^2) + \left(|V_\alpha|+|\tilde{v}_n|+|z_1|+V_x(\tilde{\eta}+\frac{\tilde{\eta}^2}{2})\right)(|e_y|+|e_x|) \tag{49}$$

By Proposition 4 the error variable $\tilde{\eta}$ is bounded. For $\dot{V}_5$ to be negative definite the bound of the error of the angle has to satisfy (48). Assuming that this condition is satisfied, it can be shown that the position errors are uniformly bounded and that the nominal dynamics of the position errors are UPAS. Furthermore, it can be seen that V_5 satisfies the conditions of Assumption 3. The conditions of Theorem 2 are satisfied and the cascaded system is UPAS on $\boldsymbol{\varphi}_7$. ■

VI. Simulation Model and Method

In this section, we will describe the high-fidelity model used to validate the system consisting of an articulated swimmer and the proposed controllers. First we describe the coupled solver algorithm used and the multi-body system (MBS) solver. Then, the implementation and some adjustments made to the controllers developed in Section V are discussed.

A. Coupled Solver

This section shortly summarizes the algorithm used to simulate a two-dimensional articulated swimmer in a complex fluid environment with fluid-structure interaction. The method is presented in [2] and relies on vortex particle-mesh (VPM) techniques coupled with a MBS solver. We first present the VPM method.

The VPM method solves the incompressible flow past deforming objects by using the velocity-vorticity formulation of the Navier-Stokes equations,

$$\frac{D\omega_f}{Dt} = (\omega_f \cdot \nabla)\boldsymbol{u}_f + \nu\nabla^2\omega_f, \tag{50a}$$

where D/Dt denotes the Lagrangian derivative, $\boldsymbol{u}_f$ is the velocity field, ν is the kinematic viscosity and ω_f is the vorticity field. The method is summarized in Algorithm 1.

The first step in Algorithm 1 consists of recovering the velocity field from the vorticity field. Then, in the projection step, the fluid evolves as if the swimmer is not present. The resulting velocity field and position of particles, $\boldsymbol{u}_f^n$ and $\boldsymbol{x}$, are then used to predict the linear and angular momentum, $\boldsymbol{P}_{\text{proj}}$ and $\boldsymbol{I}_{\text{proj}}$, of the swimmer. The resulting forces and moments are given by $\boldsymbol{F}_{\text{proj}}$ and $\boldsymbol{M}_{\text{proj}}$, respectively. The hydrodynamical forces and moments are obtained through a mapping $\mathcal{F}$ and given by $\boldsymbol{\tau}_{\text{hyd}}$, while the actuation forces are given by $\boldsymbol{\tau}_{\text{act}}$. The MBS solver then computes the generalized coordinates given by $\boldsymbol{q} = [x_1, y_1, \theta_1, \phi_1, \ldots, \phi_{N_l-1}]^T$, where N_l is the number of links, from the equations of motion. The horizontal and vertical position of the center of mass of the swimmer are given by $\boldsymbol{p}_{\text{cm}} = [x_1, y_1]^T$, while θ_1 is the absolute orientation of the first link. The relative angles between the links are given by $[\phi_1, \ldots, \phi_{N_l-1}]$. An example configuration is shown in Fig. 4. The configuration is then translated into a characteristic function that describes the swimmer's shape χ_s through the mapping $\mathcal{G}$. The velocity field of the structure is represented by $\boldsymbol{u}_s$, which is found in a similar fashion through the mapping $\mathcal{H}$. The no-slip condition is then enforced by use of Brinkman penalization in (55a), resulting in the new velocity and vorticity fields, $\boldsymbol{u}_\lambda$ and ω_λ respectively. The forces and moments resulting from constraining the fluid, $\boldsymbol{F}_{\text{pen}}$ and $\boldsymbol{M}_{\text{pen}}$, are calculated in (55c) and (55d). Finally, the vorticity field is updated in (56a). Additionally, the time-step is constrained so that $\Delta t^n \leq \min\{C, h^2/2\nu, \Delta t^{\max}\}$ where $\Delta t^n = (t^{n+1} - t^n)$, C are the Lagrangian Courant-Friedrich-Levy conditions (LCFL) [2], and h is the uniform spacing in the Cartesian discretization grid. The (LCFL) conditions may allow for time-steps that destabilize the MBS solver, therefore the time-step is constrained by a maximal time-step $\Delta t^{\max}$ which was found empirically.

B. Multibody System Solver

The equations of motion for a USR are presented in this section. A detailed model of a USR, where the full kinematics and dynamics of a planar snake robot with revolute joints are considered, is presented in [21]. The model uses Taylor's resistive [28] and Lighthill's reactive [29] models for the hydrodynamical effects on the USR. Both these models are dependent on assumptions on the flow regime and the geometry of the swimmer. Additionally, the model presented in [21] does not allow for fluid-structure interaction and the current is assumed to be constant and irrotational. Therefore, we use the coupled algorithm presented in Section VI-A, where the hydrodynamical forces and moments are generated by the computational fluid dynamics (CFD) Algorithm 1.

We define the orientation and position along the x and y-axis of link i as θ_i, x_i and y_i, respectively. Additionally, the position of the center mass of the snake robot is defined as $\boldsymbol{p}_{\text{cm}}$. The forces along the x and y-axis, and moments acting on link i, generated by the CFD, are defined as $f_{hx,i}$, $f_{hy,i}$ and $\tau_{h,i}$, respectively. Furthermore, we define $\boldsymbol{F} = [\boldsymbol{F}_x, \boldsymbol{F}_y]^T$, $\boldsymbol{F}_x = [f_{hx,1}, f_{hx,2}, ..., f_{hx,N_l}]$ and $\boldsymbol{F}_y = [f_{hy,1}, f_{hy,2}, ..., f_{hy,N_l}]$. Where N_l is the number of links.

The equations of motion are given by

$$\boldsymbol{M}_\theta\ddot{\boldsymbol{\theta}} + \boldsymbol{W}_\theta\dot{\boldsymbol{\theta}}^2 + \boldsymbol{Q}_\theta(\boldsymbol{F}) + \boldsymbol{\tau}_{\text{hyd}} = -\boldsymbol{D}^T\boldsymbol{u}, \tag{57a}$$

$$\ddot{\boldsymbol{p}}_{\text{cm}} = \frac{1}{N_l m}\begin{bmatrix}\boldsymbol{e}^T\boldsymbol{F}_x \\ \boldsymbol{e}^T\boldsymbol{F}_y\end{bmatrix}, \tag{57b}$$

where

$$\boldsymbol{M}_\theta = J\boldsymbol{I}_{Nl} + ml^2\boldsymbol{S}_\theta\boldsymbol{V}\boldsymbol{S}_\theta + ml^2\boldsymbol{C}_\theta\boldsymbol{V}\boldsymbol{C}_\theta, \tag{58a}$$

$$\boldsymbol{W}_\theta = ml^2\boldsymbol{S}_\theta\boldsymbol{V}\boldsymbol{C}_\theta - ml^2\boldsymbol{C}_\theta\boldsymbol{V}\boldsymbol{S}_\theta, \tag{58b}$$

$$\boldsymbol{Q}_\theta(\boldsymbol{F}) = \begin{bmatrix}-l\boldsymbol{S}_\theta\boldsymbol{K}\boldsymbol{F}_x \\ l\boldsymbol{C}_\theta\boldsymbol{K}\boldsymbol{F}_y\end{bmatrix}, \tag{58c}$$

$$\boldsymbol{V} = \boldsymbol{A}^T(\boldsymbol{D}\boldsymbol{D}^T)^{-1}\boldsymbol{A}, \tag{58d}$$

$$\boldsymbol{K} = \boldsymbol{A}^T(\boldsymbol{D}\boldsymbol{D}^T)^{-1}\boldsymbol{D}. \tag{58e}$$

The matrices with the subscript θ are dependent on $\boldsymbol{\theta}$, the functional argument is omitted to conserve space. The equations are on the same form as presented in [30] for land-based

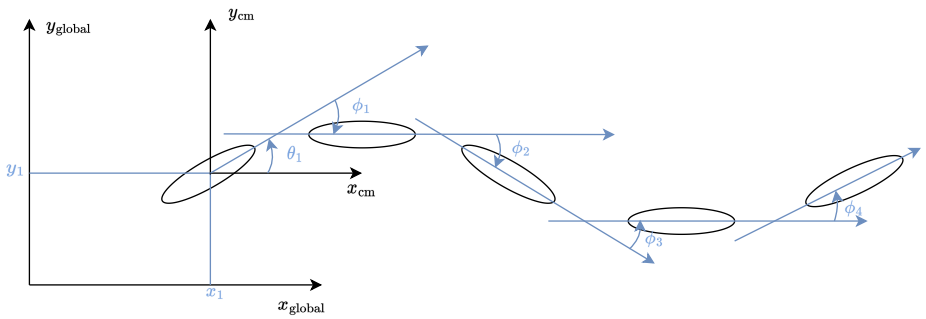

Fig. 4: Configuration of swimmer with five links.

Algorithm 1 Coupled Solver

While: $t^n \leq t^{\text{End}}$

1: Retrieve velocity field from vorticity field by solving the Poisson equation

$$\nabla^2 \boldsymbol{u}_f^n = -\nabla \times \omega_f^n. \tag{51}$$

2: Calculate projection forces and moments

$$\boldsymbol{P}_{\text{proj}}^{n+1} = \int_\Omega \rho_f \chi_s^n \boldsymbol{u}_f^n d\boldsymbol{x}, \qquad \boldsymbol{F}_{\text{proj}}^{n+1} = \frac{\boldsymbol{P}_{\text{proj}}^{n+1} - \boldsymbol{P}_{\text{proj}}^{n}}{\Delta t^n}, \tag{52a}$$

$$\boldsymbol{I}_{\text{proj}}^{n+1} = \int_\Omega \rho_f \chi_f^n (\boldsymbol{x} \times \boldsymbol{u}_f^n) d\boldsymbol{x}, \quad \boldsymbol{M}_{\text{proj}}^{n+1} = \frac{\boldsymbol{I}_{\text{proj}}^{n+1} - \boldsymbol{I}_{\text{proj}}^{n}}{\Delta t^n}. \tag{52b}$$

3: Time integration of MBS and update swimmer position and velocity

$$\boldsymbol{\tau}_{\text{hyd}}^{n+1} = \mathcal{F}(\boldsymbol{F}_{\text{proj}}^{n+1} + \boldsymbol{F}_{\text{pen}}^{n}, \boldsymbol{M}_{\text{proj}}^{n+1} + \boldsymbol{M}_{\text{pen}}^{n}), \tag{53a}$$

$$\boldsymbol{\tau}_{\text{act}}^{n+1} \rightarrow \text{provided by a control law}, \tag{53b}$$

MBS solver computes $\boldsymbol{q}^{n+1}$ and $\dot{\boldsymbol{q}}^{n+1}$ for $t^{n+1} = t^n + \Delta t^n$ with the forces calculated.

$$\chi_s^{n+1} = \mathcal{G}(\boldsymbol{q}^{n+1}), \quad \boldsymbol{u}_s^{n+1} = \mathcal{H}(\boldsymbol{q}^{n+1}, \dot{\boldsymbol{q}}^{n+1}). \tag{54a}$$

4: Penalization of vorticity field and calculation of penalization forces and moments

$$\boldsymbol{u}_\lambda^{n+1} = \frac{\boldsymbol{u}^n + \lambda_f \Delta t^n \chi_s^{n+1} \boldsymbol{u}_s^{n+1}}{1 + \lambda_f \Delta t^n \chi_s^{n+1}}, \tag{55a}$$

$$\omega_\lambda = \nabla \times \boldsymbol{u}_\lambda^{n+1}, \tag{55b}$$

$$\boldsymbol{F}_{\text{pen}}^{n+1} = \int_\Omega \lambda_f \rho_f \chi_s^{n+1} (\boldsymbol{u}_\lambda^{n+1} - \boldsymbol{u}_s^{n+1}) d\boldsymbol{x}, \tag{55c}$$

$$\boldsymbol{M}_{\text{pen}}^{n+1} = \int_\Omega \lambda_f \rho_f \chi_s^{n+1} \boldsymbol{x} \times (\boldsymbol{u}_\lambda^{n+1} - \boldsymbol{u}_s^{n+1}) d\boldsymbol{x}. \tag{55d}$$

5: Time integration of vorticity field

$$\frac{\partial \omega_\lambda}{\partial t} = \nu \nabla^2 \omega_\lambda - \nabla \cdot (\boldsymbol{u}_\lambda \omega_\lambda) \tag{56a}$$

$$\omega_f^{n+1} = \omega_\lambda^{n+1} \tag{56b}$$

End while.

snake robots, however, hydrodynamical forces and moments from the CFD are used instead of friction forces. The length, mass and moment of inertia of the links are given by l, m and J, respectively.

The orientation of each link is transformed to the generalized coordinates used in the CFD given by $\bar{\phi} = [q_3, q_4, ..., q_{n_q}]^T$. The transformation is given by

$$\bar{\phi} = \boldsymbol{H}_\phi^{-1} \boldsymbol{\theta}, \tag{59}$$

where

$$\boldsymbol{H}_\phi = \begin{bmatrix} 1 & 0 & \dots & 0 & 0 \\ 1 & 1 & \dots & 0 & 0 \\ \vdots & & \ddots & & \vdots \\ 1 & 1 & \dots & 1 & 0 \\ 1 & 1 & \dots & 1 & 1 \end{bmatrix} \in \mathbb{R}^{N \times N}. \tag{60}$$

The position of the center of mass of each link can be found through the transformation

$$\boldsymbol{p} = \begin{bmatrix} \boldsymbol{x} \\ \boldsymbol{y} \end{bmatrix} = \begin{bmatrix} -l\boldsymbol{K}^T \cos \boldsymbol{\theta} + \boldsymbol{e} q_1 \\ -l\boldsymbol{K}^T \sin \boldsymbol{\theta} + \boldsymbol{e} q_2 \end{bmatrix}, \tag{61}$$

where $\boldsymbol{x} = [x_1, x_2, \dots, x_{N_l}]^T$, $\boldsymbol{y} = [y_1, y_2, \dots, y_{N_l}]$ and $\boldsymbol{\theta} = [\theta_1, \theta_2, \dots, \theta_{N_l}]$. Furthermore, the heading of the USR is taken to be the average orientation of the links

$$\bar{\theta} = \frac{1}{N_l} \sum_{i=1}^{N_l} \theta_i. \tag{62}$$

C. Controller Adjustments for Implementation

The control-oriented model (10) approximates the complex model presented in [21]. The drag coefficients in the normal and tangential directions are assumed to be constant, and the added mass effects and nonlinear drag are assumed to be negligible. Furthermore, the orientation of each link is approximated as the forward direction of the USR, which may be a poor approximation during sharp turns and operation in conditions with significant disturbances. These assumptions may lead to poor performance if the controllers presented in Section V are implemented directly. Therefore, we make slight adjustments to the controllers to improve performance.

The joint controller, velocity controller, and attitude controller all rely on canceling parts of the dynamics, including the tangential and normal drag coefficients c_t and c_n. In the high-fidelity simulations, however, we see that these cancellations lead to worse performance. A probable cause for this can be that in the high-fidelity simulations, the drag coefficients

are likely to be time-varying or we may not have knowledge about the exact values. In addition, the cancellation terms are designed to perfectly match with a simplified model. Therefore we removed these cancellations when the controllers were implemented for the high-fidelity simulation. After making this change, significant deviations from the desired forward velocity still occurred. We hypothesize that this was due to the assumption of perfect cancellation in the analysis, together with unmodelled dynamics, which were not included in the control-oriented model. To combat this, an integral effect was included in the velocity controller in the high-fidelity simulations.

The attitude controller derived in Section V-D requires knowledge of the current and desired angular jerk and desired angular snap. Calculating these values would only be possible with knowledge of higher-order derivatives of the high-fidelity model, which is not available. Furthermore, the heading of the high-fidelity model is given by the average orientation of the links (62), and therefore we expect this to be a smoother input the more links the swimmer has. In our simulations the swimmer has few links, resulting in a fast-changing signal. The fast-changing signal with the controller presented in Section V-D results in high-frequency oscillations in the control input, which is not desirable. To combat these problems, we use the turning angle $g_2(\phi_0)$ directly as input instead of the second derivative $\ddot{\phi}_0$. Then, a third-order low-pass filter (LPF) is implemented to approximate the average input $\hat{g}_2(\phi_0)$ and the approximated derivatives $\dot{\hat{g}}_2(\phi_0)$ and $\ddot{\hat{g}}_2(\phi_0)$, as these are still required for the joint controller references. Analysis of the attitude controller with the new input is given in Appendix D.

VII. Simulation Study of Control-Oriented Model

In this section we present simulation results and discuss the performance of the controller. First, we will use the control-oriented model as simulation model, to validate the theoretical results in the ideal case.

A. Simulation Setup

The control-oriented model (10) with the controllers presented in (13), (19) and (30), was implemented in MATLAB2020B. The analytical expressions for the time derivatives of the attitude reference signal are not used due to complicated calculations and long expressions. Instead, a third order low-pass filter is used to approximate these signals. The velocities of the currents along the x and y-axis, is given by $V_x = -0.08 m/s$ and $V_y - 0.2\sin(0.2t) m/s$. Incorporating this change into the the analysis is a theoretical gap that might be addressed in future research. The parameters used are given in Table I.

B. Simulation Results

Fig. 5a and Fig. 5b show that the USR converges to a desired position along the x-axis while oscillating about the desired y-position. Note that the amplitude of the oscillations can be reduced or increased by tuning the parameters φ_7. This is shown in Figure 5a, where three cases have been plotted with different values for k. It can be observed that as k increases the amplitude decreases, as expected from the UPAS properties. The path of the USR is shown in Fig. 5c. Furthermore, from Fig. 5d it can be seen that the norm of the input is bounded. The plot also includes a close up of the input signal, showing that it is continuous and oscillatory. The velocity is shown in Fig. 5e, with an excerpt showing that the velocity reaches the reference after approximately $2s$. While the analysis gave only practical stability properties for the system, there is no visible deviation from the desired value. This might be due to either the gain being high or the nonvanishing perturbation u_ϕ being small, resulting in a very small deviation from the desired value. The angular velocity, shown in Fig. 5f, is slower and requires roughly $100s$ to reach the desired value. This might be due to the attitude error being dependent on both the velocity and relative joint angle error. These errors are high in the first few time-steps, which may be the cause of the angular velocity deviating. Another reason could be the use of a low-pass filter to approximate the time-derivatives of the reference angular velocity, since it takes time before the output from the low-pass filter becomes a good approximation.

VIII. Simulation Study High-fidelity Simulation

A. High-Fidelity Simulation Setup

This section presents the parameters used during the high-fidelity simulation. The Reynolds number is selected as $Re = 100$ for all simulations with a computational domain size given by $[0.0, 2.0]m \times [0.0, 1.0]m$ with a discretization grid resolution of $[512, 256]$. The current along the x-axis is constant and given by $-0.5 m/s$, while the current along the y-axis is time-varying and set to $-0.01\sin(0.1t) m/s$. The initial position of the USR is set to $[0.50, 0.525]$. The remaining parameters used in the simulations are given in Table II. The swimmer dimensions are illustrated in Fig. 6, where the length and width from the center are given by a and b, respectively. The length from the tip of the ellipse to the rotational joint is given by c. The kinematic viscosity is given by $\nu = \frac{V_m(2a)}{Re}$, where V_m is the maximal tangential velocity reference. In our case, we calculate that with the given initial position and gains for the guidance law, the forward velocity reference varies between $[-0.16, 0.16] m/s$. For positions further away from the desired position, it would be beneficial to saturate the desired velocity, due to it being dependent on the distance to the desired position. See Fig. 7 for a snapshot of the simulation of the swimmer moving into position.

B. High-Fidelity Simulation Results

The USR slowly converges to the desired position along the x-axis over about $50s$ as can be seen in Fig. 8b. The position deviates a little from its desired value and is also not held as steadily compared to the simulation of the simplified model, shown in Fig. 5b. This is not unexpected, as there are more disturbances and unmodelled dynamics present in the high-fidelity simulation. The position along the y-axis is shown in Fig. 8a, where it can be seen that it oscillates about its desired setpoint, similarly to the results from the simulation

TABLE I: Simulation parameters for ideal case

N_l	m	c_t	c_n	c_p	λ_1	λ_2	α	$\gamma_1(i)$	$K_{\phi,1}$
10	1.56	4.45	17.3	35.7	6	120	$7\ cm$	1	3
$K_{\phi,2}$	$K_{\lambda,1}$	$K_{\lambda,2}$	K_R	K_1	K_2	K_3	k	δ	$\phi_{0,\max}$
6	2	2	1	2	1	1	0.05	$40°$	$40°$

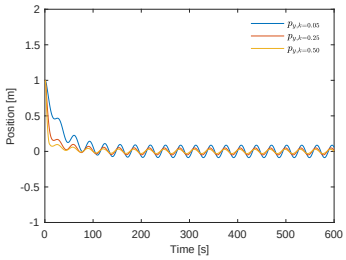

(a) Position along y-axis of the USR.

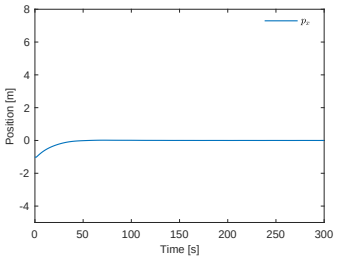

(b) Position along x-axis of the USR.

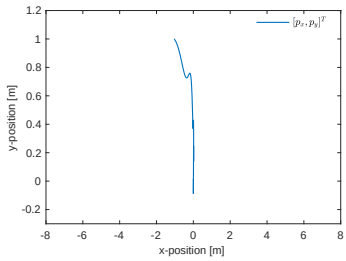

(c) Position of USR.

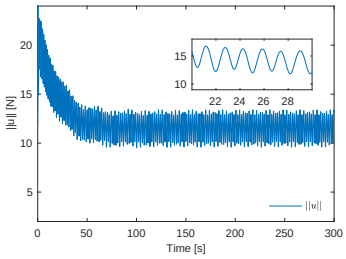

(d) Norm of input.

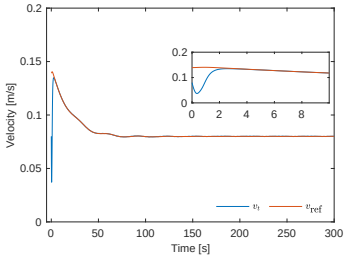

(e) Tangential relative velocity v_t and desired tangential relative velocity V_d.

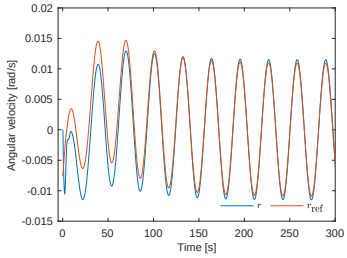

(f) Angular velocity r and desired angular velocity r_d.

Fig. 5: Simulation results of the simplified control-oriented model.

of the simplified model in Fig. 5a. Furthermore, we see that increasing the gain k_y results in smaller oscillations about the desired value, which is a property of UPAS. The deviation is greater in the y-position than in x, due to the unknown time-varying current. Like in the position along the x-axis, we see high-frequency oscillation also in the position along y-axis. The tangential velocity is shown in Fig. 8c, and a closer plot of the first $50s$ is shown in Fig. 8d. It can be seen that the tangential velocity tracks the desired velocity well. While it does oscillate about the desired value, this is expected in a complex environment, and the maximal deviation is approximately $0.02m/s$. The angular velocity is shown in Fig. 8e, and a close-up showing the first $50s$ is shown in Fig. 8f. While there are large deviations from the desired angular velocity, the desired and actual angular velocities appear to oscillate about the same average value. These deviations may also be why the positions along the x- and y-axis also have high-frequency oscillations. The deviations are expected since the heading of the USR is defined as the average heading of the links, and the simulated swimmer only has 8 links. We hypothesize that increasing the number of links would yield better performance. Additionally, the input used for the attitude controller is processed through a third-order LPF as mentioned in Section VI-C, which gives an averaging effect in the input to angular velocity, while also introducing some phase-shift.

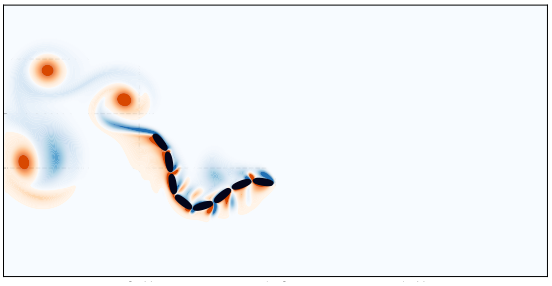

Fig. 7: Snapshot from the high-fidelity simulation of the USR showing fluid-structure interaction.

This may also contribute to the observed deviations.

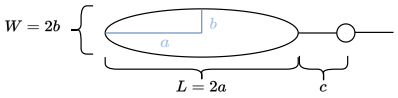

Fig. 6: Link and joint configuration.

IX. Conclusions

Previous work has established sufficient conditions for uniform global practical asymptotic stability (UGPAS) and

TABLE II: Simulation parameters high-fidelity simulation

N_l	a	b	c	ρ_f	ρ_s	λ_f	$\Delta t^{\max}$	$K_{\phi,1}$
8	$0.03125m$	$0.2a$	$0.01m$	$997kg/m^2$	$997kg/m^2$	10^4	$0.001s$	2
$K_{\phi,2}$	$K_{\lambda,1}$	$K_{\lambda,2}$	K_R	K_1	λ_1	λ_2	m	δ
2	1000	2000	200	100	6	120	$0.61kg$	$60°$
k_x	k_y	c_t	c_n	c_p	$\phi_{0,\max}$	$\gamma_1(i)$	α	
0.1	0.2	4.45	17.3	35.7	$20°$	1	$40°$	

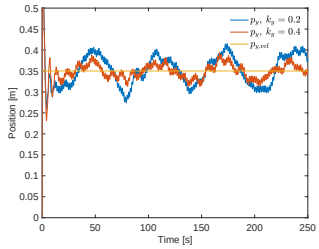

(a) Position along y-axis of the USR in high-fidelity simulation.

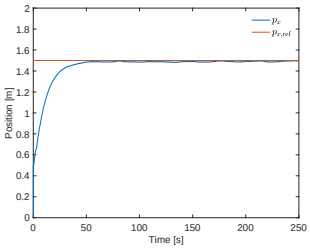

(b) Position along x-axis of the USR in high-fidelity simulation.

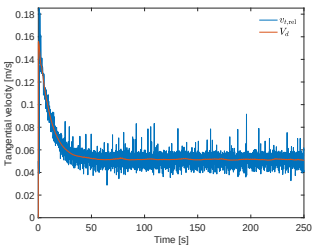

(c) Actual and desired tangential relative velocity of the USR.

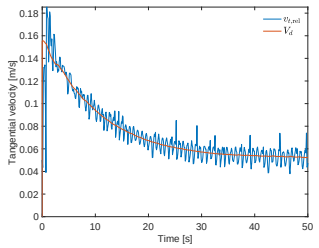

(d) Actual and desired tangential velocity of the USR, zoomed in.

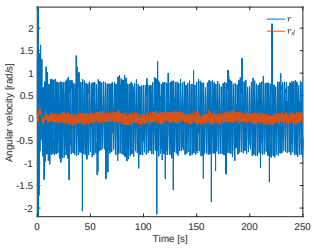

(e) Actual and desired angular velocity of the USR.

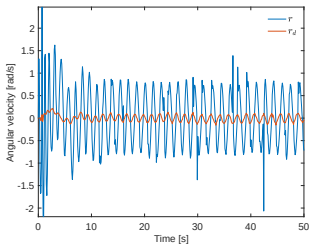

(f) Actual and desired angular velocity of the USR, zoomed in.

Fig. 8: Results from the high-fidelity simulation study.

uniform semi-global practical asymptotic stability (USPAS) for nonlinear time-varying dynamical and cascaded systems. To our knowledge, there are no results for a local adaptation of UPAS for cascaded systems. Therefore, Lyapunov sufficient conditions for UPAS are provided, and it is proven that the UPAS property is retained in cascaded systems.

This is used to design a controller that allows a USR to achieve some desired position in the presence of time-varying disturbances while moving against a constant current along the x-axis. The system with the designed controller is proven to be UPAS on the set of parameters. Furthermore, the theoretical results are verified through a simulation study, both in the ideal case matching a simplified model and through high-fidelity simulations with a coupled solver to capture the fluid-structure interaction. The results from the simulation study with high-fidelity simulations and adaptations to the controllers indicate that there are some deviations in the tracking of angular velocity and tangential velocity. However, the position of the USR reaches the desired position along the x-axis, and oscillates about the desired position along the y-axis, overall matching the behavior of the ideal case quite well.

APPENDIX

A. Proof of Theorem 1

The proof follows directly from the proof of Theorem 10 in [16], Proposition 2 in [31] and Theorem 7.11 in [32], by setting Δ_1 to be constant. The complete proof is provided here for completeness. For a UPAS system, the region of attraction is not required to be adjustable by choice of parameter. Therefore the proof has to be adapted to the case where it is not required that Δ can be arbitrarily enlarged. Let $\Delta > 0$ be a positive constant and choose $\Delta > \delta > 0$ such that

$$\underline{\alpha}_\delta^{-1} \circ \overline{\alpha}_\delta(\delta) < \Delta. \tag{63}$$

Let V_δ and $\theta^*(\delta)$ be generated by the assumptions. Then applying Lemma 7.6 from [32] to V_δ, with $k = 1$, ensures the existence of a continuously differentiable function $\mathcal{V}_\delta$ and class $\mathcal{K}$-functions $\underline{\chi}_\delta$ and $\overline{\chi}_\delta$ such that for all $x \in X$, with $X = H(\delta, \Delta)$, and all $t \in \mathbb{R}_{\geq 0}$

$$\underline{\chi}_\delta(|x|) \leq \mathcal{V}_\delta(t,x) \leq \overline{\chi}_\delta(|x|) \tag{64}$$

$$\frac{\partial \mathcal{V}_\delta}{\partial t}(t,x) + \frac{\partial \mathcal{V}_\delta}{\partial x}(t,x) f(t,x,\theta) \leq -k\mathcal{V}_\delta(t,x) \tag{65}$$

where

$$\underline{\chi}_\delta^{-1} \circ \overline{\chi}_\delta(s) = \underline{\alpha}_\delta^{-1} \circ \overline{\alpha}_\delta(s), \ \forall s \geq 0 \tag{66}$$

It then follows from (5) that

$$\lim_{\delta\to 0} \underline{\chi}_\delta^{-1} \circ \overline{\chi}_\delta(\delta) = 0. \tag{67}$$

Furthermore, inverting (66) yields

$$\overline{\chi}_\delta^{-1} \circ \underline{\chi}_\delta(s) = \overline{\alpha}_\delta^{-1} \circ \underline{\alpha}_\delta(s),\ \forall s \geq 0 \tag{68}$$

Then by selecting $a = \delta$ and $b = \Delta$ the requirements for uniform boundedness as presented in Proposition 23 in [18] are satisfied and we get that

$$|x_0| \leq \bar{\Delta} \Longrightarrow |x(t)| \leq \Delta,\ \forall t \geq t_0, \tag{69}$$

where $\bar{\Delta} := \overline{\chi}_\delta^{-1} \circ \underline{\chi}_\delta(\Delta)$. This shows that solutions of initial states in a ball $\mathcal{B}_{\bar{\Delta}}$ never escape $\mathcal{B}_\Delta$. Applying Lemma 28 from [18] with $X = H(\delta, \Delta)$, $k = 1$ and $c = 0$ to (65) gives that for any $x_0 \in \mathcal{B}_{\bar{\Delta}}$ and all $t_0 \in \mathbb{R}_{\geq 0}$

$$|x(t)| \leq \underline{\alpha}_\delta^{-1} \circ \overline{\alpha}_\delta(\delta) + \underline{\alpha}_\delta^{-1}\left(\overline{\alpha}_\delta(|x_0|)e^{-(t-t_0)}\right). \tag{70}$$

Defining

$$\beta_\delta(s,t) := \underline{\alpha}_\delta^{-1}\left(\overline{\alpha}_\delta(s)e^{-t}\right), \tag{71}$$

$$\bar{\delta} := \underline{\alpha}_\delta^{-1} \circ \overline{\alpha}_\delta(\delta), \tag{72}$$

implying that $\forall x_0 \in \mathcal{B}_{\bar{\Delta}}$ and $\forall t_0 \in \mathbb{R}_{\geq 0}$ the solution satisfies

$$|x(t)| \leq \bar{\delta} + \beta_\delta(|x_0|, t - t_0). \tag{73}$$

It can be seen that $\beta_\delta(|x_0|, t - t_0)$ is a class $\mathcal{KL}$ function and from (67) that $\bar{\delta}$ can be arbitrarily diminished by choice of δ, and by extension parameters θ.

B. Proof of Proposition 1

The main part of this proof consists of showing that solutions of (6) starting sufficiently close to the origin do not exit the ball $\mathring{\mathcal{B}}_{\Delta_0}$. Then, since by assumption the right-hand side of (6) is locally Lipschitz everywhere in the state space, by [26, Theorem 3.3] solutions starting at some time t_0 and which lie entirely in the compact set $\bar{\mathcal{B}}_{\Delta_0}$ are defined for all time $t \geq t_0$, completing the statement (9).

We will prove that solutions of (6) starting sufficiently close to the origin do not exit $\mathring{\mathcal{B}}_{\Delta_0}$ by contradiction. Let Assumptions 1-3 be satisfied, and assume that for any Δ_0, any δ_1, any δ_2 and any $\gamma > 0$, there exist solutions of (6) with $\theta = \theta^*$, generated by δ_1, δ_2, starting from initial conditions $x_0 \in \mathring{\mathcal{B}}_\gamma$ and which cross the boundary of $\mathring{\mathcal{B}}_{\Delta_0}$. The parameter θ^* consists of $\theta_1^* = \theta_1^*(\delta_1)$ generated by Assumption 3 and $\theta_2^* \in D_{f_2}(\delta_2, \Delta_2) \cap \Theta_2$. In other words, for any Δ_0, any δ_1 and any δ_2, there are solutions of (6), with $\theta = \theta^*$, starting arbitrarily close to the origin which reach the boundary of $\mathring{\mathcal{B}}_{\Delta_0}$. Then we can construct a sequence of initial conditions $\left(x_n^0\right)_{n\in\mathbb{N}} \subset \mathring{\mathcal{B}}_{\Delta_0}$, $\lim_{n\to\infty} x_n^0 = 0$ where for each n, there exists an initial time $t_n^0 \geq 0$ and a finite $T_n > 0$ such that the solution of (6) starting in x_n^0 at time t_n^0 reaches the boundary of $\mathring{\mathcal{B}}_{\Delta_0}$ after a time interval T_n, i.e.

$$\begin{aligned} &t_n^0 \leq t < t_n^0 + T_n \ \Rightarrow\ |x(t, t_n^0, x_n^0, \theta^*)| < \Delta_0, \\ &|x(t_n^0 + T_n, t_n^0, x_n^0, \theta^*)| = \Delta_0 \end{aligned} \tag{74}$$

Since we assume (74) has to hold for any Δ_0, let $\Delta_0 < \min(\Delta_1, \Delta_2)$, where Δ_2 and Δ_1 follow from by Assumptions 2 and 3, respectively.

Now, we make use of the system properties similarly to the reasoning in the stability proof in [18]. Consider a function V_{δ_1} generated by Assumption 3, and let Lemma 27 in [18] with $X = H(\delta_1, \Delta_1)$ and with the choice $k = 1$ generate a function $\mathcal{V}_{\delta_1}$, class $\mathcal{K}$ functions $\underline{\chi}_{\delta_1}$, $\overline{\chi}_{\delta_1}$, and a continuous nondecreasing function d_{δ_1} such that$\forall x \in X$ and $\forall t \in \mathbb{R}_{\geq 0}$

$$\underline{\chi}_{\delta_1}(|x|) \leq \mathcal{V}_{\delta_1}(t,x) \leq \overline{\chi}_{\delta_1}(|x|) \tag{75a}$$

$$\frac{\partial \mathcal{V}_{\delta_1}}{\partial t}(t,x) + \frac{\partial \mathcal{V}_{\delta_1}}{\partial x}(t,x) f(t,x) \leq -\mathcal{V}_{\delta_1}(t,x) \tag{75b}$$

$$\left|\frac{\partial \mathcal{V}_{\delta_1}}{\partial x}(t,x)\right| \leq d_{\delta_1}(|x|) \tag{75c}$$

hold for $\mathcal{V}_{\delta_1}$, for some $\delta_1 < \Delta_0$. From [18, Lemma 27], we have that for any $s \in \mathbb{R}_{\geq 0}$

$$\underline{\chi}_{\delta_1}^{-1} \circ \overline{\chi}_{\delta_1}(s) = \underline{\alpha}_{\delta_1}^{-1} \circ \overline{\alpha}_{\delta_1}(s). \tag{76}$$

The Lie derivative of $\mathcal{V}_{\delta_1}$ with $\theta = \theta^*$ yields

$$\dot{\mathcal{V}}_{\delta_1} = \frac{\partial \mathcal{V}_{\delta_1}}{\partial t} + \frac{\partial \mathcal{V}_{\delta_1}}{\partial x_1}(f_1(t, x_1, \theta_1^*) + g(t, x, \theta^*)x_2). \tag{77}$$

Then $\forall x_1 \in H(\delta_1, \Delta_1)$ and $\forall t \geq 0$

$$\dot{\mathcal{V}}_{\delta_1} \leq -\mathcal{V}_{\delta_1} + \left|\frac{\partial \mathcal{V}_{\delta_1}}{\partial x_1}\right| |g(t, x, \theta^*)||x_2|, \tag{78a}$$

$$\leq -\mathcal{V}_{\delta_1} + d_{\delta_1}(|x_1|)G(|x|)|x_2|. \tag{78b}$$

Let $x_i(t, x_n^0) := x_i(t, t_n^0, x_n^0, \theta^*)$ for $i = 1, 2$, and $v_{\delta_1,\Delta_1}(t, x_n^0) := \mathcal{V}_{\delta_1,\Delta_1}(t, x_1(t, x_n^0))$. Since $x_n^0 \in \mathcal{B}_{\Delta_0} \subset \mathcal{B}_{\Delta_2}$, by Assumption 2 there exists a class $\mathcal{KL}$ function β_2 s.t.

$$|x_2(t, x_n^0)| \leq \beta_2(|x_2(t_n^0, x_n^0)|, t - t_n^0) + \delta_2 \quad \forall t \geq t_n^0 \tag{79}$$

holds for any $\delta_2 < \Delta_2$. Now define

$$\Gamma_n := \left\{t \in [t_n^0, t_n^0 + T_n] \ \middle|\ \delta_1 \leq |x_1(t, x_n^0)| \leq \Delta_1\right\}. \tag{80}$$

Note that by (74) and since $\delta_1 < \Delta_0 \leq \Delta_1$, the set Γ_n is nonempty (since it contains at least $t_n^0 + T_n$, and by continuity of solutions some interval preceding that).

Combining (78), (74) and (79), we have that $\forall t \in \Gamma_n$,

$$\begin{aligned} \dot{v}_{\delta_1}(t, x_n^0) &\leq -v_{\delta_1}(t) \\ &\quad + d_{\delta_1}(\Delta_1)G(\Delta_0)\left(\beta_2(|x_2(t_n^0, x_n^0)|, t - t_n^0) + \delta_2\right) \\ &\leq -v_{\delta_1}(t) + c_3(|x_n^0|) \end{aligned} \tag{81}$$

where

$$c_3(\cdot) = d_{\delta_1}(\Delta_1)G(\Delta_1)\left(\beta_2(\cdot, 0) + \delta_2\right). \tag{82}$$

Integrating (81) over Γ_n in the same manner as is done in the proof of Lemma 28 in [18], and writing $x(t_n^0 + T_n, x_n^0)$ for $x(t_n^0 + T_n, t_n^0, x_n^0, \theta^*)$, we have

$$\begin{aligned} |x(t_n^0 + T_n, x_n^0)| &\leq \delta_1 + \underline{\alpha}_{\delta_1}^{-1}\left(\overline{\alpha}_{\delta_1}(\delta_1) + c_3(|x_n^0|)\right) \\ &\quad + \underline{\alpha}_{\delta_1}^{-1}\left(\overline{\alpha}_{\delta_1}(|x_n^0|)e^{-T_n} + c_3(|x_n^0|)\right) \\ &\leq \delta_1 + \underline{\alpha}_{\delta_1}^{-1}\left(\overline{\alpha}_{\delta_1}(\delta_1) + c_3(|x_n^0|)\right) \\ &\quad + \underline{\alpha}_{\delta_1}^{-1}\left(\overline{\alpha}_{\delta_1}(|x_n^0|) + c_3(|x_n^0|)\right). \end{aligned} \tag{83}$$

Define

$$\delta_3 := \delta_1 + \underline{\alpha}_{\delta_1}^{-1}\left(\overline{\alpha}_{\delta_1}(\delta_1) + c_3(0)\right) + \underline{\alpha}_{\delta_1}^{-1}\left(c_3(0)\right), \tag{84}$$

$$\eta(s) := \underline{\alpha}_{\delta_1}^{-1}\left(\overline{\alpha}_{\delta_1}(\delta_1) + c_3(s)\right) + \underline{\alpha}_{\delta_1}^{-1}\left(\overline{\alpha}_{\delta_1}(s) + c_3(s)\right) - \underline{\alpha}_{\delta_1}^{-1}\left(\overline{\alpha}_{\delta_1}(\delta_1) + c_3(0)\right) - \underline{\alpha}_{\delta_1}^{-1}\left(c_3(0)\right), \tag{85}$$

where, since c_3 is a continuous nonincreasing function, η is a class $\mathcal{K}$ function. By Assumptions 2 and 3, we can choose δ_1, δ_2 respectively, to generate corresponding parameters θ_1^*, θ_2^* such that $\delta_3 < \Delta_0 - 2\varepsilon$ for some $\varepsilon > 0$. Furthermore, since η is a class $\mathcal{K}$ function and $\lim_{n\to\infty} x_n^0 = 0$, we can find an N such that $\eta(|x_n^0|) < \varepsilon\ \forall n \geq N$. This gives

$$|x(t_n^0 + T_n, t_n^0, x_n^0, \theta^*)| \leq \Delta_0 - \varepsilon \neq \Delta_0\ \forall n \geq N \tag{86}$$

which contradicts (74). Taking $\gamma < \eta^{-1}(\epsilon)$, for a $\Delta_0 < \min(\Delta_1, \Delta_2)$, we have thus found a δ_1, δ_2 and γ such that no solution starting from $x_0 \in \mathring{\mathcal{B}}_\gamma$ can exit $\mathring{\mathcal{B}}_{\Delta_0}$.

C. Proof of Theorem 2

The proof of Theorem 2 follows from the proof of Theorem 13 in [18] by setting Δ_1 to be constant.

Consider $\mathcal{V}_{\delta_1}$ as given by (75). For any δ_1 that satisfies $\Delta_1 > \delta_1 > 0$ it follows from (5) and (76) that

$$\lim_{\delta_1 \to 0} \underline{\chi}_{\delta_1}^{-1} \circ \overline{\chi}_{\delta_1}(\delta_1) = 0. \tag{87}$$

Define $\Delta := \min\{\Delta_1, \Delta_2, \gamma\}$ where γ is given by Proposition 1. Choose any $\theta_1^* \in \Theta_1$ satisfying Assumption 3 and $\theta_2^* \in D_{f_2}(\delta_2, \Delta_2) \cap \Theta_2$ such that Proposition 1 holds. We first show that there exists a positive δ_3 such that the ball $\mathcal{B}_{\delta_3}$ is uniformly stable by constructing $\eta \in \mathcal{K}$ such that $\forall \boldsymbol{x}_0 \in \mathcal{B}_\Delta$

$$|x_1(t, t_0, x_0, \delta)|_{\delta_3} \leq \eta(|x_0|). \tag{88}$$

We use this property to prove that a ball larger than $\mathcal{B}_{\delta_3}$, is uniformly attractive (UA) on $\mathcal{B}_\Delta$ and we construct a $\mathcal{KL}$ estimate for the solutions. Finally, we show that the estimates of the ball to which solutions converge can be arbitrarily diminished. The time derivative of $\mathcal{V}_{\delta_1}$ with $\theta = \theta^*$ is given by (77).

Additionally, we define the subset

$$\Gamma := \{t \geq t_0 \ \mid\ \delta_1 \leq |x_1(t, t_0, x_0, \theta^*)| \leq \Delta_1\}. \tag{89}$$

We now use $x_1(t)$ for $x_1(t, t_0, x_0, \theta^*)$ and $v_{\delta_1}(t)$ for $\mathcal{V}_{\delta_1}(t, x_1(t))$. We then have $\forall x_0 \in \mathcal{B}_\Delta, \forall t \in \Gamma$,

$$\dot{v}_{\delta_1}(t) \leq -v_{\delta_1}(t) + d_{\delta_1}(\Delta_1) G(\Delta_1) |x_2(t)|. \tag{90}$$

Like previously, since by Assumption 1 the driving system (6b) is UPAS, there is a class $\mathcal{KL}$ function

$$|x_2(t)| \leq \beta_2(|x_{20}|, t - t_0) + \delta_2, \forall t \geq 0. \tag{91}$$

for $x_{20} \in \mathcal{B}_{\Delta_2}$. It follows that $\forall x_0 \in \mathcal{B}_\Delta$ and $\forall t \in \Gamma$

$$\dot{v}_{\delta_1}(t) \leq -v_{\delta_1}(t) + d_{\delta_1}(\Delta_1) G(\Delta_1) \left(\beta_2(|x_{20}|, t - t_0) + \delta_2\right), \tag{92}$$

which implies that

$$\dot{v}_{\delta_1}(t) \leq -v_{\delta_1}(t) + c_3(|x_0|),\ \forall x(t) \in H(\delta_1, \Delta_1), \tag{93}$$

where c_3 is the same function as defined by (82).

We now consider Lemma 28 in [18], which allows us to construct a bound with $V = \mathcal{V}_{\delta_1}$, $k = 1$, $c = c_3(|x_0|)$ and $X = H(\delta, \Delta)$. In view of Proposition 1, we have that $\forall x_0 \in \mathcal{B}_\Delta$ and $\forall t_0 \in \mathbb{R}_{\geq 0}$

$$|x(t)| \leq \delta_1 + \underline{\alpha}_{\delta_1}^{-1}\left(\overline{\alpha}_{\delta_1}(\delta_1) + c_3(|x_0|)\right) + \underline{\alpha}_{\delta_1}^{-1}\left(\overline{\alpha}_{\delta_1}(|x_0|) + c_3(|x_0|)\right). \tag{94}$$

Defining δ_3 and a function η as given by (84) and (85), respectively, we conclude that, for any $x_0 \in \mathcal{B}_\Delta$ and all $t_0 \in \mathbb{R}_{\geq 0}$ it holds that

$$|x_1(t)|_{\delta_3} \leq \eta(|x_0|),\ \forall t \geq t_0. \tag{95}$$

Uniform stability of $\mathcal{B}_{\delta_3}$ on $\mathcal{B}_\Delta$ follows by noticing that η is a class $\mathcal{K}$ function. To show uniform attractivity of a ball, we again consider (92).

Because β_2 is a class $\mathcal{KL}$ function, there is a time $t_1 \geq 0$ such that

$$\beta_2(\Delta, t - t_0) \leq \delta_2,\ \forall t \geq t_0 + t_1. \tag{96}$$

Therefore it is implied that

$$\dot{v}_{\delta_1} \leq -v_{\delta_1}(t) + 2d_{\delta_1}(\Delta_1) G(\Delta_1) \delta_2,\ \forall t \geq t_0 + t_1. \tag{97}$$

Applying Lemma 28 [18] again, it follows that for any $x_0 \in \mathcal{B}_\Delta$, all $t_0 \in \mathbb{R}_{\geq 0}$ and all $t \geq t_0 + t_1$

$$|x(t)|_{\delta_1} \leq \underline{\alpha}_{\delta_1}^{-1}(\overline{\alpha}_{\delta_1}(\delta_1) + 2d_{\delta_1}(\Delta_1) G(\Delta_1)\delta_2) + \underline{\alpha}_{\delta_1}^{-1}\left(\overline{\alpha}_{\delta_1}(\Delta_1) e^{-(t - t_0 - t_1)} + 2d_{\delta_1}(\Delta_1) G(\Delta_1)\delta_2\right). \tag{98}$$

We define

$$t_2 := t_1 + \ln\left(\frac{\overline{\alpha}_{\delta_1}(\Delta_1)}{\overline{\alpha}_{\delta_1}(\delta_1)}\right). \tag{99}$$

By inserting (99) and defining

$$\delta_4 := \delta_1 + 2\underline{\alpha}_{\delta_1}^{-1}\left(\overline{\alpha}_{\delta_1}(\delta_1) + 2d_{\delta_1}(\Delta_1) G(\Delta_1)\delta_2\right), \tag{100}$$

we get the following bound;

$$|x_1(t, t_0, x_{10})|_{\delta_4} = 0,\ \forall t \geq t_0 + t_2. \tag{101}$$

Meaning that the set is uniformly attractive. Furthermore, it can be seen that $\delta_3 \leq \delta_4$ from equation (84) and (100). Let

$$\delta := \max\{\delta_2, \delta_4\}, \tag{102}$$

Then we see that from (95) it is implied that $|x_1(t)|_\delta \leq \eta(|x_0|),\ \forall t \geq t_0$. Furthermore, by considering (101) the following bound can be found $\forall t \geq t_0,\ \forall x_0 \in \mathcal{B}_\Delta$

$$|x_1(t)| \leq \delta + \eta(|x_0|) e^{-(t - t_0 - t_2)}. \tag{103}$$

Recalling that t_2 is not dependent on t_0 or x_0, and defining

$$\beta(s, t) := \max\left(\eta(s) e^{-(t - t_2)}, \beta_2(s, t)\right), \tag{104}$$

we can conclude that for any $x_0 \in \mathcal{B}_\Delta$

$$|x(t)| \leq \delta + \beta(|x_0|, t - t_0), \tag{105}$$

because this is a class $\mathcal{KL}$ function, we conclude that $\mathcal{B}_\delta$ is UAS on $\mathcal{B}_\Delta$. To show that δ can be arbitrarily diminished, consider (5) in Assumption 3, while recalling that d_{δ_1}, G and $\underline{\chi}_{\delta_1}$ are independent of δ_2. Then δ_4 and by extension δ_3 can be made arbitrarily diminished by choice of δ_1 and δ_2. Hence it is sufficient to pick the parameters $\theta_1^* \in \Theta_1$ and $\theta_2^* \in \Theta_2$ generated by the chosen δ_1 and δ_2 to conclude that for any δ satisfying $\Delta > \delta > 0$, there exists some parameters such that $\mathcal{B}_\delta$ is UAS on $\mathcal{B}_\Delta$.

D. Analysis of the Modified Guidance Law and Attitude Controller

An analysis of the modified guidance law and attitude controller used in the high-fidelity simulations is given here. Consider (10f) and define the control input $u_\theta = g_2(\phi_0)$. We can then write

$$\dot{r} = -\lambda_1 r + \lambda_2 V_d u_\theta + g_\theta(\lambda, t, \tilde{\boldsymbol{\phi}}, z_1), \tag{106}$$

where

$$g_\theta(\lambda, t, \tilde{\boldsymbol{\phi}}, z_1) = \lambda_2 V_d \alpha_1(\lambda) + g_3(t, \tilde{\boldsymbol{\phi}}, z_1). \tag{107}$$

Because $g_3(t, \tilde{\boldsymbol{\phi}}, z_1)$ is bounded as explained in Section V-D, V_d is bounded by design and $\alpha_1(\lambda)$ is a vector of sin-functions, we can define the following bound

$$g_\theta(\lambda, t, \tilde{\boldsymbol{\phi}}, z_1) \leq G_\theta. \tag{108}$$

We then select the input as

$$u_\theta = \frac{1}{\lambda_2 V_d}(\lambda_1 r_d - K_\theta \tilde{r} + \dot{r}_d - K_R e_R). \tag{109}$$

By inserting (109) into (106), we obtain:

$$\dot{y}_1 = -(\lambda_1 + K_\theta) y_1 + g_\theta(\lambda, t, \tilde{\boldsymbol{\phi}}, z_1) - K_R e_R. \tag{110}$$

We define $\boldsymbol{x}_\phi := [e_R, y_1]^T$, $\boldsymbol{\varphi}_\phi = [K_1, K_R]^T$ and $\boldsymbol{\varphi}_5' = [\boldsymbol{\varphi}_\phi, \boldsymbol{\varphi}_1]^T$. Combining (110), (26) and (32b), gives

$$\dot{\boldsymbol{x}}_\phi = \boldsymbol{f}_\phi(t, \boldsymbol{x}_\phi, \boldsymbol{\varphi}_\phi) + \boldsymbol{g}_3(t, \boldsymbol{x}_4), \tag{111a}$$
$$\dot{\boldsymbol{x}}_4 = \boldsymbol{f}_4(t, \boldsymbol{x}_4, \boldsymbol{\varphi}_1). \tag{111b}$$

We then make the following propositions:

Proposition 8: Consider a system given by (10) and the controller (109) and assume that the initial conditions satisfy

$$\Psi(\boldsymbol{R}(0), \boldsymbol{R}_d(0)) < 2, \tag{112a}$$
$$y_{10}^2 < 2K_R(2 - \Psi(\boldsymbol{R}(0), \boldsymbol{R}_d(0))). \tag{112b}$$

Then for sufficiently small values of $\tilde{\boldsymbol{\phi}}$ and z_1 and by selecting K_θ such that

$$\frac{G_\theta}{(\lambda_1 + K_\theta)} << 2K_R \tag{113}$$

it can be shown that $\Psi(\boldsymbol{R}(0), \boldsymbol{R}_d(0)) \in L_2 \ \forall t$.

Proof: Define the Lyapunov function $V_{\theta,1} = \frac{1}{2}y_1^2 + K_R\Psi(\boldsymbol{R}, \boldsymbol{R_d})$. By differentiating and inserting (109) and (108), we get

$$\dot{V}_{\theta,1} \leq -(\lambda_1 + K_\theta) y_1^2 + G_\theta y_1. \tag{114}$$

By selecting the gains as in (113), the Lyapunov function is negative definite when approaching the circle with radius $2K_R$. Implying that if the initial conditions satisfy (112), the states are bounded away from $\beta_r \ \forall t$. ■

Proposition 9: Consider a system given by (10) with the controller (109) and the guidance law described in Section V-D. By selecting K_θ and K_R such that

$$K_R > \frac{\lambda_1 + K_\theta}{2} \tag{115}$$

and assuming that the bounds given by (113) are satisfied, the system is UPAS on the set of parameters $\boldsymbol{\varphi}_5'$.

Proof: The proof follows along the lines of the proof for Proposition 5. Consider the bounds given by (37), and the Lyapunov function $V_{\theta,2} = V_{\theta,1} + \beta_\phi e_R y_1$. By using the bounds (37), we show that the Lyapunov function is bounded by

$$\boldsymbol{x}_\phi^T \boldsymbol{M}_{\theta,1} \boldsymbol{x}_\phi \leq V_{\theta,2} \leq \boldsymbol{x}_\phi^T \boldsymbol{M}_{\theta,2} \boldsymbol{x}_\phi, \tag{116}$$

where $\boldsymbol{M}_{\theta,1} = \frac{1}{2}\begin{bmatrix} K_R & -\beta_\phi \\ -\beta_\phi & 1 \end{bmatrix}$, $\boldsymbol{M}_{\theta,2} = \frac{1}{2}\begin{bmatrix} \frac{2K_R}{2-\psi_\phi} & \beta_\phi \\ \beta_\phi & 1 \end{bmatrix}$. Selecting $\beta_\phi < \sqrt{K_R}$, the eigenvalues of $\boldsymbol{M}_{\theta,1}$ and $\boldsymbol{M}_{\theta,2}$ are positive, and the following bounds can be used

$$\lambda_m(\boldsymbol{M}_{\theta,1})||\boldsymbol{y}_\theta||^2 \leq V_{\theta,2} \leq \lambda_M(\boldsymbol{M}_{\theta,2})||\boldsymbol{y}_\theta||^2. \tag{117}$$

The derivative of the Lyapunov function is then bounded by

$$\begin{aligned} \dot{V}_{\theta,2} \leq & -(\lambda_1 + K_\theta) y_1^2 + G_\theta y_1 + \beta_\phi C y_1^2 \\ & + \beta_\phi e_R(-(\lambda_1 + K_\theta) y_1 + G_\theta - K_R e_R), \end{aligned} \tag{118}$$

$$\begin{aligned} \dot{V}_{\theta,2} \leq & -((\lambda_1 + K_\theta)(1 - \frac{1}{2}\beta_\phi) - \beta_\phi C)|y_1| - G_\theta)|y_1| \\ & - \beta_\phi((K_R - \frac{\lambda_1 + K_\theta}{2})|e_R| - G_\theta)|e_R|. \end{aligned} \tag{119}$$

Now select

$$\beta_\phi < \min\left\{ \frac{(\lambda_1 + K_\theta)}{\lambda_1 + K_\theta + C}, \sqrt{K_R}, \ 2 \right\}, \tag{120}$$

and the gains according such that (115) holds. Then the nominal part of the dynamics (110) is UPAS by Theorem 1. The system (111) then satisfies Assumption 1-3 and by Theorem 2 the cascaded system is UPAS on the set of parameters $\boldsymbol{\varphi}_5'$. ■

REFERENCES

[1] E. Kelasidi, P. Liljebäck, K. Y. Pettersen, and J. T. Gravdahl, "Innovation in underwater robots: Biologically inspired swimming snake robots," *IEEE Robot. Automat. Mag.*, vol. 23, no. 1, pp. 44–62, 2016.

[2] C. Bernier, M. Gazzola, R. Ronsse, and P. Chatelain, "Simulations of propelling and energy harvesting articulated bodies via vortex particle-mesh methods," *J. Comput. Phys.*, vol. 392, pp. 34–55, Sep 2019.

[3] C. Bernier, M. Gazzola, P. Chatelain, and R. Ronsse, "Numerical simulations and development of drafting strategies for robotic swimmers at low reynolds number," in *Proc. IEEE Int. Conf. Biomed. Robot. Biomechatron.*, Enschede, The Netherlands, Aug. 2018.

[4] P. Liljebäck, I. U. Haugstuen, and K. Y. Pettersen, "Path following control of planar snake robots using a cascaded approach," *IEEE Trans. Control Syst. Technol.*, 2011.

[5] E. Kelasidi, P. Liljebäck, K. Y. Pettersen, and J. T. Gravdahl, "Integral line-of-sight guidance for path following control of underwater snake robots: Theory and experiments," *IEEE Trans. Robot.*, vol. 33, no. 3, pp. 610–628, Jun. 2017.

[6] A. M. Kohl, K. Y. Pettersen, E. Kelasidi, and J. T. Gravdahl, "Planar path following of underwater snake robots in the presence of ocean currents," *IEEE Robot. Autom. Lett.*, vol. 1, no. 1, pp. 383–390, Jan. 2016.

[7] E. Rezapour, A. Hofmann, K. Y. Pettersen, A. Mohammadi, and M. Maggiore, "Virtual holonomic constraint based direction following control of planar snake robots described by a simplified model," in *Proc. IEEE Conf. Control Appl.*, Antibes, France, Oct. 2014.

[8] M. I. El-Hawwary and M. Maggiore, "Reduction theorems for stability of closed sets with application to backstepping control design," *Automatica*, vol. 49, no. 1, pp. 214–222, Jan. 2013.

[9] A. Mohammadi, E. Rezapour, M. Maggiore, and K. Y. Pettersen, "Maneuvering control of planar snake robots using virtual holonomic constraints," *IEEE Trans. Control Syst. Technol.*, vol. 24, no. 3, pp. 884–899, May 2016.

[10] A. M. Kohl, K. Y. Pettersen, and J. T. Gravdahl, "Velocity and orientation control of underwater snake robots using absolute velocity feedback," in *IEEE Conf. Control Technol. Appl.*, Maui, HI, USA, Aug. 2017.

[11] T. Lee, "Geometric tracking control of the attitude dynamics of a rigid body on SO(3)," in *Proc. Am. Control Conf.*, San Francisco, CA, USA, Jun. 2011.

[12] T. Lee, M. Leok, and N. H. McClamroch, "Geometric tracking control of a quadrotor UAV on SE(3)," in *Proc. IEEE Conf. Decision Control*, Atlanta, GA, USA, Dec. 2010.
[13] C. Paliotta and K. Y. Pettersen, "Geometric path following with ocean current estimation for ASVs and AUVs," in *Proc. Am. Control Conf.*, Boston, MA, USA, Oct. 2016.
[14] E. Sontag, "Remarks on stabilization and input-to-state stability," in *Proc. IEEE Conf. Decision Control*, Tampa, FL, USA, Dec. 1989.
[15] E. Panteley and A. Loría, "Growth rate conditions for uniform asymptotic stability of cascaded time-varying systems," *Automatica*, vol. 37, no. 3, pp. 453–460, 2001.
[16] A. Chaillet and A. Loría, "Uniform global practical asymptotic stability for time-varying cascaded systems," *Eur. J. Control*, vol. 12, no. 6, pp. 595–605, 2006.
[17] M. Vidyasagar, "Decomposition techniques for large-scale systems with nonadditive interactions: Stability and stabilizability," *IEEE Trans. Autom. Control*, vol. 25, no. 4, pp. 773–779, 1980.
[18] A. Chaillet and A. Loría, "Uniform semiglobal practical asymptotic stability for non-autonomous cascaded systems and applications," *Automatica*, vol. 44, no. 2, pp. 337–347, 2008.
[19] R. Kristiansen, A. Loria, A. Chaillet, and P. J. Nicklasson, "Uniform practical output-feedback stabilization of spacecraft relative rotation," in *Proc. 2008 Am. Control Conf.* IEEE, 2008, pp. 4862–4867.
[20] A. Orucevic, J. T. Gravdahl, K. Y. Pettersen, and A. Chaillet, "Uniform practical asymptotic stability for position control of underwater snake robots," in *Proc. 2022 IEEE Conf. Control Technol. Appl.*, Trieste, Italy, Aug. 2022.
[21] E. Kelasidi, K. Y. Pettersen, J. T. Gravdahl, and P. Liljebäck, "Modeling of underwater snake robots," in *Proc. IEEE Int. Conf. Robot. and Autom.*, Hong Kong, China, May 2014.
[22] P. Liljebäck, K. Y. Pettersen, Ø. Stavdahl, and J. T. Gravdahl, "Lateral undulation of snake robots: a simplified model and fundamental properties," *Robotica*, vol. 31, no. 7, pp. 1005–1036, Apr. 2013.
[23] E. Kelasidi, K. Y. Pettersen, and J. T. Gravdahl, "A control-oriented model of underwater snake robots," in *Proc. IEEE Int. Conf. Robot. Biomim.*, Bali, Indonesia, Dec. 2014.
[24] A. M. Kohl, E. Kelasidi, K. Y. Pettersen, and J. T. Gravdahl, "A control-oriented model of underwater snake robots exposed to currents," in *Proc. IEEE Conf. Control Appl.*, Sydney, Australia, Sep. 2015.
[25] A. M. Kohl, K. Y. Pettersen, E. Kelasidi, and J. T. Gravdahl, "Analysis of underwater snake robot locomotion based on a control-oriented model," in *Proc. Conf. Robot. Biomim.*, Zhuhai, China, Dec. 2015, pp. 1930–1937.
[26] H. K. Khalil, *Nonlinear systems*, 3rd ed. Prentice-Hall, 2002.
[27] V. I. Arnold, *Mathematical Methods of Classical Mechanics*. Springer New York, 1989.
[28] G. I. Taylor, "Analysis of the swimming of long and narrow animals," *Proc. R. Soc. A: Math. Phys. Eng. Sci.*, vol. 214, no. 1117, pp. 158–183, 1952.
[29] M. J. Lighthill, "Large-amplitude elongated-body theory of fish locomotion," *Proc. R. Soc. B: Biol. Sci.*, vol. 179, no. 1055, pp. 125–138, 1971.
[30] P. Liljebäck, K. Y. Pettersen, and Ø. Stavdahl, "Modelling and control of obstacle-aided snake robot locomotion based on jam resolution," in *Proc. 2009 IEEE Int. Conf. Robot. Autom.* IEEE, 2009, pp. 3807–3814.
[31] A. Chaillet and A. Loría. (2006) Uniform global practical asymptotic stability for time-varying cascaded systems. [Online]. Available: https://arxiv.org/abs/math/0503039v2
[32] A. Chaillet, "On stability and robustness of nonlinear systems applications to cascaded systems," Ph.D. dissertation, Paris-Sud University, 2006.

Amer Orucevic (GS'22) Received the MSc degree in cybernetics and robotics from the Norwegian University of Science and Technology (NTNU), Trondheim, in 2020, where he is currently pursuing a PhD in engineering cybernetics. His current research interests include nonlinear control of underwater snake robots, and energy-efficient locomotion.

Marianna Wrzos-Kaminska received the MSc degree in engineering cybernetics from the Norwegian University of Science and Technology (NTNU), Trondheim, in 2018, where she is currently pursuing a PhD in engineering cybernetics. Her current research interests include nonlinear control of articulated intervention-AUVs.

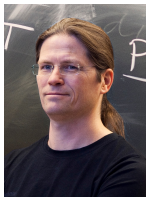

Jan Tommy Gravdahl (Senior Member, IEEE) received the Siv.ing. and Dr.ing. degrees in engineering cybernetics from the Norwegian University of Science and Technology (NTNU), Trondheim, Norway, in 1994 and 1998, respectively. Since 2005, he has been a Professor with the Department of Engineering Cybernetics, NTNU, where he also served as the Head of Department, from 2008 to 2009. He has supervised the graduation of 150 M.Sc. and 14 Ph.D. candidates. He has published five books and more than 250 articles in international conferences and journals. His current research interests include mathematical modeling and nonlinear control in general, in particular applied to turbomachinery, marine vehicles, spacecraft, robots, and high-precision mechatronic systems. Prof. Gravdahl was a recipient of the IEEE Transactions on Control Systems Technology Outstanding Paper in 2000 and 2017. Since 2017, he has been a Senior Editor of the IFAC Journal Mechatronics, where he also served as an Associate Editor since 2016, and since 2020, he has been an Associate Editor of the IEEE Transactions on Control Systems Technology. He has been on the editorial board and IPC for numerous international conferences.

Kristin Y. Pettersen (S'93-M'98-SM'04-F'17)received the MSc and PhD degrees in engineering cybernetics from the Norwegian University of Science and Technology (NTNU), Trondheim, Norway, in 1992 and 1996, respectively. She is a Professor in the Department of Engineering Cybernetics, NTNU, where she has been a faculty member since 1996. She was Head of Department 2011-2013, Vice-Head of Department 2009-2011, and Director of the NTNU ICT Program of Robotics 2010-2013. She is Adjunct Professor at the Norwegian Defence Research Establishment (FFI). In the period 2013 – 2022 she is also Key Scientist at the CoE Centre for Autonomous Marine Operations and Systems. She is a co-founder of the NTNU spin-off company Eelume AS, where she was CEO 2015-2016.

She has published four books and more than 300 papers in international journals and conference proceedings. Her research interests focus on nonlinear control of mechanical systems with applications to robotics, with a special emphasis on marine robotics and snake robotics. She was awarded the IEEE Transactions on Control Systems Technology Outstanding Paper Award in 2006 and in 2017. She was awarded an ERC-AdG-2020 Advanced Grant from the European Research Council, and received the IEEE CSS Hendrik W. Bode Lecture Prize in 2020.

She is currently an elected member of the IEEE Control Systems Society Board of Governors and a member of the IFAC Council and the EUCA Council. She has also held several board positions in industrial and research companies. She has served as Associate Editor of IEEE Control Systems Magazine, as Associate and Senior Editor of IEEE Transactions on Control Systems Technology as well as Co-Editor-in-Chief for IFAC Mechatronics. She is IEEE CSS Distinguished Lecturer 2019-2022, IEEE Fellow, member of the Norwegian Academy of Technological Sciences, and member of the Academy of the Royal Norwegian Society of Sciences and Letters.